

CHAPTER 1

PHASE TRANSITIONS IN THE PSEUDOSPIN-ELECTRON MODEL

Ihor Stasyuk

*Institute for Condensed Matter Physics
of the National Academy of Science of Ukraine
1 Svientsitskii Str., UA-79011 Lviv, Ukraine
E-mail: ista@icmp.lviv.ua*

A review of the present state of investigations of the pseudospin-electron model (PEM), which is used in the theory of strongly correlated electron systems, is given. The model is used to describe the systems with the locally anharmonic elements of structure represented in the model by pseudospins. The consideration is based on the dynamical mean field theory approach and the generalized random phase approximation. Electron spectrum and thermodynamics of the model are investigated; the cases of the simplified model, the model with strong interaction and the two-sublattice model are studied more in detail. The phase transitions into other uniform or modulated states as well as superconducting phases are described; the criteria of their realization are established. Based on this, the description of structural and dielectric (ferroelectric type) instabilities, phase separation and bistability phenomena is given. A comparison is made with the thermodynamics of the Falicov-Kimball model (which can be considered as a particular case of PEM). The possibility of applying the PEM to the analysis of thermodynamics of the real HTSC systems is discussed. Attention is paid to the unsolved problems in the study of PEM.

Contents

1	Introduction	2
2	Thermodynamics of Simplified PEM in Dynamical Mean Field Theory	5
3	Simplified PEM in Generalized Random Phase Approximation	13
3.1	Strong Coupling Case; $U = 0$, $\Omega = 0$	13
3.1.1	Thermodynamics of the Uniform State	13
3.1.2	The Chess-Board Phase	20

3.2	Weak Coupling Case; $U = 0$	26
3.2.1	Uniform Phase	26
3.2.2	Phase with Double Modulation	31
3.2.3	Pair Correlation Function and Susceptibilities	34
3.3	Superconductivity in the PEM	39
4	Thermodynamics of PEM at Finite U Values; the $U \rightarrow \infty$ Limit	42
5	Two-Sublattice Pseudospin-Electron Model	49
6	Conclusions	56
	Acknowledgements	58
	References	58

1. Introduction

Much attention is paid in recent years to the investigation of systems with strong electron correlations, such as crystalline compounds with the transition and rare-earth ions (transition metals, transition metal oxides, mixed valent compounds, heavy fermion systems, high temperature superconductors, etc.). Their specific electronic, magnetic and conducting properties as well as the presence of a variety of phase transitions and the phenomena that are connected with this property are caused to a great extent by the splitting and reconstruction of energy spectrum due to correlation effects. The theory of such systems is based on the Hubbard model and on its generalizations, where the crucial idea is the one concerning the decisive role of the strong short-range interaction of particles (electrons). At the presence of additional (i.e., vibrational) degrees of freedom, one can mention, among others, the pseudospin-electron model (PEM). The model appeared recently in connection with the investigation of the high- T_c superconductors. It was introduced to describe the contribution of locally-anharmonic elements of the crystal structure to their electronic properties.

Electron system in PEM is described by the Hubbard Hamiltonian while the anharmonic vibrational modes are treated using the pseudospin formalism. The model Hamiltonian is as follows

$$H = \sum_i [U n_{i,\uparrow} n_{i,\downarrow} + (g S_i^z - \mu)(n_{i,\uparrow} + n_{i,\downarrow}) - h S_i^z - \Omega S_i^x] + \sum_{i,j,\sigma} t_{ij} a_{i,\sigma}^+ a_{j,\sigma}. \quad (1)$$

Here $a_{i,\sigma}$, $a_{i,\sigma}^+$ are electron annihilation and creation operators, $n_{i,\sigma}$ is an electron occupation number; besides the electron correlation (U -term), the single-site part includes the interaction with pseudospin (g -term) and the energy of the tunnelling-like splitting of vibrational levels (Ω -term); the field h describes the asymmetry of local potential. The electron transfer (t -term) is included as well.

The pseudospin-electron Hamiltonian (in form (1) with inclusion only of the g -interaction) was used by Müller with the aim of describing the anharmonic vibrations in the oxygen subsystem of the high- T_c superconducting crystals of the YBaCuO type.¹ The YBa₂Cu₃O_{7- δ} crystal is a typical and most studied example of such objects. The unit cell contains, besides two superconducting planes, the chain (at the $\delta \ll 1$ composition) elements Cu₁-O₁, connected by Cu₁-O₄-Cu₂ bridges with Cu₂-O₂ plains through the apical oxygen ions O₄. The vibrations of these ions along the c -axis (perpendicularly to the plains) exhibit a strong anharmonicity. Much evidence exists in support of this concept. One can mention the EXAFS data,^{2,3} Raman scattering and dielectric measurements,^{4,5,6,7,8,9} local polaron phenomena,^{10,11} bistabilities in the normal phase region¹² as well as neutron scattering investigations¹³ or the results of the first principle LAPW calculations.¹⁴ Despite a certain ambiguity in the data, the conclusions were made about the existence of two different equilibrium positions of the O₄ ion. The local double-well picture as an approximate simplified model was supported by the oxygen O₄ vacancy effect on the positions of apical ions observed in Ref. [15].

Moreover, a connection between positions of O₄ ions and electron states in Cu₂-O₂ plains plays an important role in YBa₂Cu₃O_{7- δ} crystals. The data given in Ref. [16] point to the existence of a significant correlation between the occupancy of electron states of the Cu₂ ion and the R_{O₄-Cu₂} distance as well as to the decrease of this distance at the transition from the metallic orthorhombic phase to the semiconducting one (that takes place at $\delta > \delta^* = 0.55$). These and other similar facts suggest the presence of a large electron-vibrational coupling. In the pseudospin representation, when the pseudospin variable $S_i^z = \pm 1/2$ defines the positions of O₄ ions, it is described by the $gS_i^z n_{i\sigma}$ term.

Consideration based on the PEM was applied to the HTSC systems starting from Refs. [1,17–20]. Hamiltonian similar to (1) was used by Hirsch and Tang in the study of electron states in the framework of cluster calculations. In the context of the idea concerning the effect of anharmonicity on the superconducting transition temperature,^{17,18,19,21} the possible connection between superconducting pairing and the lattice anharmonicity was considered by Frick et al.²² (the quantum Monte-Carlo calculations). In what follows, the investigations of the PEM were devoted to the analysis of the electron spectrum,²³ the pseudospin and collective dynamics,^{24,25} the charge and pseudospin pair correlations and the behaviour of dielectric susceptibility.²⁶

In subsequent investigations, the main attention was paid to the thermodynamics of the model in special cases and simplifications: (i) a model with the infinitely large correlation ($U \rightarrow \infty$) when the double occupation of electron states on the site is excluded; (ii) simplified PEM with $U = 0$ and $\Omega = 0$; (iii) simplified model ($U = 0$) with the tunnelling-like dynamics ($\Omega \neq 0$); (iv) two-sublattice PEM for the layered structures of the YBaCuO-type; (v) the cluster PEM of ferroelectric-superconductor heterostructures.^{27,28}

There was performed a study of phase transitions between the states with different electron concentrations and with different orientations of pseudospins (in the regime of the fixed chemical potential, $\mu = \text{const}$), and the phase separation effects at a given concentration of electrons ($n = \text{const}$).^{29,30} The possibility of the appearance of a doubly modulated (so-called chessboard) phase or an incommensurate phase (in the case of weak coupling) was established;^{31,32,33} the superconducting instability in PEM was analysed.³⁴ In the case of two-sublattice PEM the structural instabilities of the ferroelectric type as well as the bistability phenomena were revealed and analysed.^{35,36,37,38} The study of the PEM thermodynamics was performed mainly within the generalized random phase approximation (GRPA).³⁹ A method of dynamical mean field theory (DMFT) was used in the case of simplified PEM,²⁹ when the analytic formulation of the theory is possible.

As was shown, the PEM also possesses an interesting collective dynamics of pseudospins. The corresponding spectrum changes its form depending on the electron concentration and temperature;^{24,25} the spectrum is different at high or small values of g and its shape also depends on the h and Ω parameters. In Refs. [40–42], the contributions into Raman scattering intensity, connected with the mentioned collective pseudospin excitations (that correspond to the phonon-like vibrations of anharmonic subsystems in the YBaCuO structures) and electron intraband and interband transitions, were considered.

The PEM is closely related to the Falicov-Kimball (FK) model intensively studied in recent years (see, for example, Ref. [43]), in which the interaction between the localized and itinerant particles (electrons) is responsible for the similar phase transitions (between states with different concentrations of particles and with/without spatial modulation). The simplified version of PEM corresponds to the FK model in case there is no tunnelling-like splitting in the PEM and when the localized and the moving particles in FK model have different chemical potentials (one can pass

to FK model putting $S_i^z = w_i - 1/2$ and $h = \tilde{\mu}$, where w_i and $\tilde{\mu}$ are occupation number and chemical potential of localized particles, respectively). The regimes of thermodynamic averaging are usually different for both models (a fixed concentration of the localized particles for FK model and a given value of the field h for the PEM).

It should be mentioned that for the recent few years the PEM has found application in describing the charge transfer in molecular and crystalline systems with hydrogen bonds.⁴⁴ The model is also very promising in investigating the thermodynamics of processes connected with ionic intercalation in the layered structures (see Ref. [45]), where different separated positions exist in the unit cell for the intercalate ion, and the hopping between them is possible (intercalation of Li^+ ions in the TiO_2 matrix provides an example of such a situation⁴⁶). A specific version of PEM was recently used⁴⁷ in modelling the electronic properties and the field effect in the $\text{CuO}_2/\text{SrTiO}_3$ interfaces in HTSC/STO heterostructures.

This paper presents a review of the main results concerning the thermodynamics and energy spectrum of the PEM in the above mentioned cases and approximations. The case of the simplified PEM ($U = 0$; $\Omega = 0$ or $\Omega \neq 0$) is considered more in detail. Dynamic properties of PEM are not considered here. An attention is paid to the possible application of the PEM to the description of inhomogeneous states, structural instabilities and bistability phenomena as well as transitions into the phases with the charge modulation in the high T_c superconductors and other systems to which the model can be applied.

2. Thermodynamics of Simplified PEM in Dynamical Mean Field Theory

The dynamical mean field theory approach proposed by Metzner and Vollhardt⁴⁸ for the Hubbard model (see also Ref. [49] and references therein) is a nonperturbative scheme which is exact in the limit of the infinite space dimension ($d \rightarrow \infty$). The method is very successful in considering the systems with strong electron correlations and is used with advantage in solving a variety of problems and models. Within the framework of DMFT, investigations of the single-particle spectrum and the thermodynamics of the simplified PEM were performed for a strong coupling case ($g \gg W$, where W is the half-width of the initial electron band).²⁹ The Fourier-transform $G_\sigma(\omega_n, \mathbf{k})$ of the electron Green's function

$$G_{ij}^\sigma(\tau - \tau') = -\langle T a_{i\sigma}(\tau) a_{j\sigma}^\dagger(\tau') \sigma(\beta) \rangle_0 / \langle \sigma(\beta) \rangle_0, \quad (2)$$

(where T denotes the τ -ordering procedure) with the scattering matrix

$$\sigma(\beta) = T \exp \left\{ - \int_0^\beta d\tau \sum_{ij\sigma} t_{ij} a_{i\sigma}^+(\tau) a_{j\sigma}(\tau) \right\} \quad (3)$$

and the averaging with the single-site part $H_0 = \sum_i H_i$ of the Hamiltonian (1), is expressed as a series in terms of the electron hopping parameter t_{ij} . The Larkin's equation

$$G_{ij}^\sigma(\tau - \tau') = \Xi_{ij}^\sigma(\tau - \tau') + \Xi_{il}^\sigma(\tau - \tau'') t_{lm} G_{mj}^\sigma(\tau'' - \tau') \quad (4)$$

separates the total irreducible (with respect to t_{ij}) part Ξ^σ ; formally

$$G_\sigma(\omega_n, \mathbf{k}) = \frac{1}{\Xi_\sigma^{-1}(\omega_n, \mathbf{k}) - t_{\mathbf{k}}}. \quad (5)$$

In the case of high dimensions ($d \rightarrow \infty$), when the hopping integral is scaled ($t_{ij} \rightarrow t_{ij}/\sqrt{d}$), only single-site contributions survive in the expression for Ξ_σ .⁵⁰

$$\Xi_{ij}^\sigma(\tau - \tau') = \delta_{ij} \Xi_\sigma(\tau - \tau'); \quad \Xi_\sigma(\omega_n, \mathbf{k}) = \Xi_\sigma(\omega_n). \quad (6)$$

Such a site-diagonal function, as it was shown by Brandt and Mielsch,⁵¹ can be calculated by mapping the infinite-dimensional lattice problem on the atomic model

$$\begin{aligned} e^{-\beta H} &\rightarrow e^{-\beta H_{\text{eff}}} = e^{-\beta H_0} \\ &\times T \exp \left\{ - \int_0^\beta d\tau \int_0^\beta d\tau' \sum_\sigma J_\sigma(\tau - \tau') a_\sigma^+(\tau) a_\sigma(\tau') \right\} \end{aligned} \quad (7)$$

with auxiliary Kadanoff-Baym field $J_\sigma(\tau - \tau')$ ⁵² which should be selfconsistently determined from the condition that the same function Ξ_σ defines the Green's functions for lattice (5) and atomic limit

$$G_\sigma^{(a)}(\omega_n) = \frac{1}{\Xi_\sigma^{-1}(\omega_n) - J_\sigma(\omega_n)}. \quad (8)$$

“Dynamical” mean field $J_\sigma(\tau - \tau')$ (so-called coherent potential) describes the hopping (transfer) of electron from atom into environment at the moment τ , and propagation in environment without stray into atom until moment τ' . The connection between this “dynamical” mean field of atomic problem and Green's function of the lattice can be obtained using standard coherent potential approximation (CPA):⁴⁹

$$J_\sigma(\omega_n) = \Xi_\sigma^{-1}(\omega_n) - G_\sigma^{-1}(\omega_n), \quad (9)$$

where

$$G_{\sigma}^{(a)}(\omega_n) = G_{\sigma}(\omega_n) = \int_{-\infty}^{+\infty} dt \frac{\rho(t)}{\Xi_{\sigma}^{-1}(\omega_n) - t} \quad (10)$$

is a single-site Green's function both for atomic limit and lattice. Here summation over wave vector was changed by the integration with the density of states (DOS) $\rho(t)$ (the Gaussian one for the hypercubic lattice $\rho(\varepsilon) = \frac{1}{W\sqrt{\pi}}e^{-\varepsilon^2/W^2}$ and semi-elliptic DOS for the Bethe lattice $\rho(\varepsilon) = \frac{2}{\pi W^2}\sqrt{W^2 - \varepsilon^2}$, see Ref. [49]).

In order to find expression for Green's function in the atomic limit, one can use the fact that the statistical operator of the single-site problem (7) can be expressed in the form²⁹

$$e^{-\beta H_{\text{eff}}} = P^+ e^{-\beta H_+} + P^- e^{-\beta H_-} \quad (11)$$

because the atomic space of states splits into two independent subspaces.

As a result, the single-electron Green's function is a sum of Green's functions in subspaces and is equal to

$$G_{\sigma}^{(a)}(\omega_n) = \frac{\langle P^+ \rangle}{i\omega_n + \mu - J_{\sigma}(\omega_n) - \frac{g}{2}} + \frac{\langle P^- \rangle}{i\omega_n + \mu - J_{\sigma}(\omega_n) + \frac{g}{2}}. \quad (12)$$

Here $\langle \dots \rangle$ is the statistical averaging with the effective Hamiltonian (7). Partition functions in subspaces are

$$\begin{aligned} Z_{\pm} &= \text{Sp} e^{-\beta H_{\pm}} = e^{\pm \frac{\beta h}{2} - Q_{\pm}} \\ &= e^{\pm \frac{\beta h}{2}} \prod_{\sigma} \left(1 + e^{-\beta(\mu \mp \frac{g}{2})} \right) \prod_n \left(1 - \frac{J_{\sigma}(\omega_n)}{i\omega_n + \mu \mp \frac{g}{2}} \right). \end{aligned} \quad (13)$$

Pseudospin mean value is determined by the equation

$$\langle S^z \rangle = \frac{1}{2} \frac{Z_+ - Z_-}{Z_+ + Z_-} = \frac{1}{2} \tanh \frac{1}{2} (\beta h - (Q_+[\langle S^z \rangle] - Q_-[\langle S^z \rangle])) . \quad (14)$$

Electron concentration mean value is determined by

$$\langle n \rangle = \frac{1}{\beta} \sum_{m\sigma} G_{\sigma}(\omega_m) \quad (15)$$

and the functional of the grand canonical potential can be derived in the standard way for DMFT

$$\frac{\Phi}{N} = \Phi_{(a)} - \frac{1}{\beta} \sum_{n\sigma} \left\{ \ln G_{\sigma}^{(a)}(\omega_n) - \frac{1}{N} \sum_{\mathbf{k}} \ln G_{\sigma}(\omega_n, \mathbf{k}) \right\}, \quad (16)$$

where

$$\Phi_{(a)} = -\frac{1}{\beta} \ln(Z_+ + Z_-) \quad (17)$$

is a thermodynamic potential for atomic problem.

The solution of the above given set of equations and the calculation of thermodynamic potential were performed for the case of semi-elliptic DOS. The field $J_\sigma(\omega_n)$ is determined by the simple cubic equation

$$J_\sigma(\omega_n) = \frac{W^2}{4} \left\{ \frac{\langle P^+ \rangle}{i\omega_n + \mu - J_\sigma(\omega_n) - \frac{g}{2}} + \frac{\langle P^- \rangle}{i\omega_n + \mu - J_\sigma(\omega_n) + \frac{g}{2}} \right\}. \quad (18)$$

The solutions with $\Im J_\sigma(\omega) > 0$ are considered; the condition $\Im J_\sigma(\omega) \rightarrow 0$ determines the band boundaries. Their dependence on coupling constant at the fixed value of $\langle S^z \rangle$ is shown in Fig. 1. It can be seen that there exists

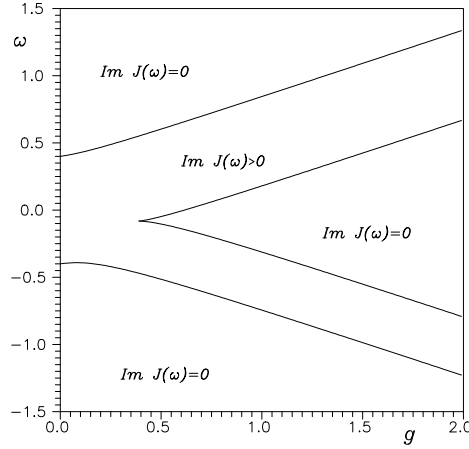


Fig. 1. Electron bands boundaries (semi-elliptic DOS, $W = 0.4$, $\langle S^z \rangle = 0.2$).

a critical value of $g \sim 0.5W$ when a gap in spectrum appears and we have an analogue of the Mott transition. In the case when the single-electron Green's function is calculated in Hubbard-I approximation (the scattering processes via coherent potential are not taken into account, $J_\sigma(\omega) = 0$ and $\Xi_\sigma(\omega_n) = \langle P^+ \rangle / (i\omega_n + \mu - g/2) + \langle P^- \rangle / (i\omega_n + \mu + g/2)$), the electron subbands are always split and the gap in spectrum exists at any values of g (see below). From this point of view, the Hubbard-I approximation is insufficient; even in the case of strong coupling ($g \gg W$) it only qualitatively describes the dependence of the subband half-widths on $\langle S^z \rangle$.²⁶

The expressions presented above allow us to investigate in the DMFT approach the thermodynamics of the simplified PEM. It was done in Ref. [26] in the $\mu = \text{const}$ and $n = \text{const}$ regimes.

In the first case, the thermodynamically stable states are determined from the minimum of the thermodynamic potential (16). Analysis of solutions of CPA equations for $J_\sigma(\omega_n)$ together with the equation (14) for $\langle S^z \rangle$ shows that in this regime the first order phase transitions with the jumps of the pseudospin mean value and electron concentration can take place. Such transitions are realized when the μ and h values correspond to the split subbands in an electron spectrum (see the phase diagram $(\mu - h)$ at $T = 0$ in Fig. 2). The field dependencies of $\langle S^z \rangle$ and grand canonical

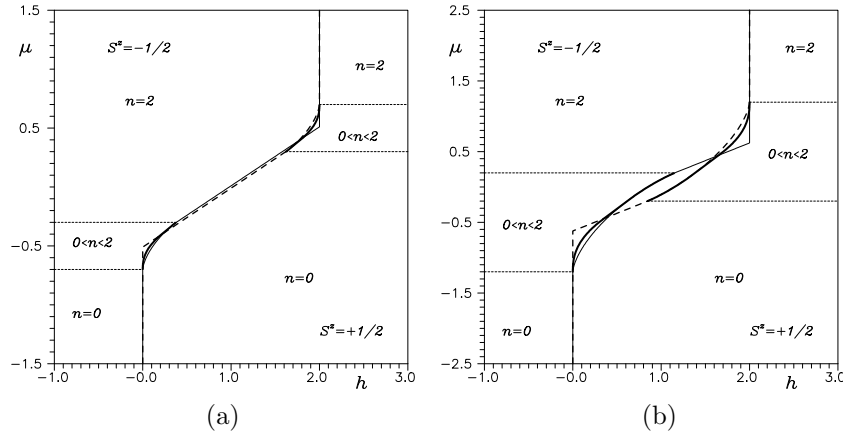


Fig. 2. Phase diagram $(\mu - h)$. Dashed and thin solid lines surround regions with $S^z = \pm \frac{1}{2}$, respectively. The lines of the first order phase transition are shown in bold. a) $g = 1$, $W = 0.2$; b) $g = 1$, $W = 0.7$.

potential Φ in the region of the phase transition point are shown in Fig. 3. Since the band structure is determined by the pseudospin mean value, the change of the latter is accompanied by the corresponding reconstruction of the electron spectrum. With the temperature increase the region of the phase coexistence narrows. The corresponding phase diagram $(T_c - h)$ is shown in Fig. 4. One can see that with respect to the Ising model the phase coexistence curve is shifted in the field and deviates from the vertical line. Hence, the possibility of the first order phase transition with the temperature change exists in the pseudospin-electron model for the narrow range of h values.

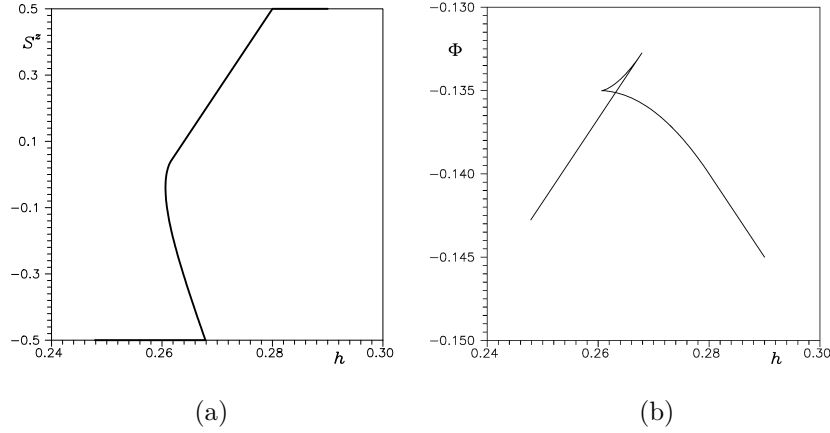


Fig. 3. Field dependencies of $\langle S_z \rangle$ (a) and grand canonical potential (b) for $\mu = \text{const}$ regime when chemical potential is placed in the lower subband $\mu = -0.37$ ($W = 0.2$, $g = 1$, $T = 0$).

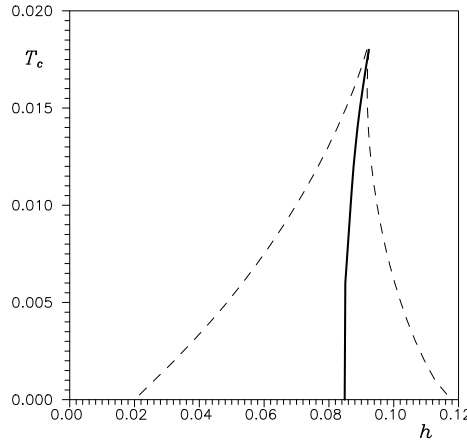


Fig. 4. Phase diagram ($T_c - h$): solid and dashed lines indicate the first order phase transition line and boundaries of the phase stability region, respectively ($g = 1$, $W = 0.2$, $\mu = -0.5$)

When the electron concentration is fixed (regime $n = \text{const}$), the first order phase transition transforms into the phase separation. The regions appear where the derivative $\partial\mu/\partial n$ is negative, Figs. 5 and 6. The corresponding phase diagram ($T - n$) is built (Fig. 7, see also Ref. [26]) with the use of the “Maxwell rule” which follows in this case from the replacement of

the original free energy in its concavity region by the tangent line. The diagram describes the separation to the states with the large and small electron concentrations (and with the $\langle S^z \rangle \approx -1/2$ and $\langle S^z \rangle \approx +1/2$ pseudospin averages at low temperatures, respectively).

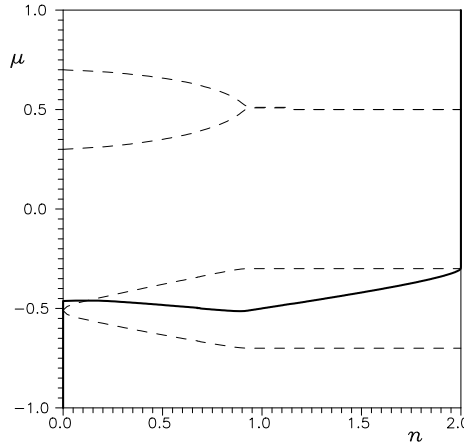


Fig. 5. Dependence of the chemical potential μ and electron bands boundaries (dashed lines) on the electron concentration n ($T = 0.001$, $g = 1$, $W = 0.2$, $h = 0.1$).

It should be noted that the problem of phase separation in strongly correlated systems is not new (see Ref. [53] and references therein). It was shown for Hubbard and $t - J$ models⁵⁴ that for some values of the parameters, the system separates into hole-rich and hole-poor regions with paramagnetic and antiferromagnetic orders, respectively. In our case of PEM without electron correlations, the system separates into regions with electron spectrum that contains both wide empty electron band and occupied localized states (at $n \sim 0$) and partially filled wide electron band and empty localized states (at $n \sim 1$), see Fig. 5; their weights are determined by the electron concentration. Localized states of such a type (polarons) result from the strong electron-pseudospin coupling (strong interaction of electrons with the out of plane apical oxygen vibrations) in the case of YBaCuO-type structures, and it can be supposed that the hopping between such polarons manifests itself in the carrier relaxation.⁵⁵

For the first time the possibility of phase separation in PEM was mentioned in Ref. [56] where it was considered within GRPA in the limit of strong correlation $U \rightarrow \infty$ (see below, Sec. 4). Here it is obtained for the

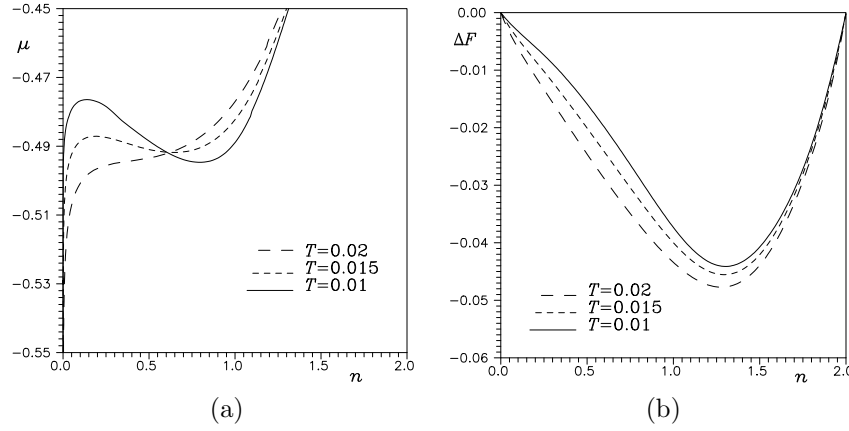


Fig. 6. Dependence of the chemical potential μ (a) and the deviation of free energy from linear dependence $\Delta F = F(n) - \frac{n}{2}F(2) - (1 - \frac{n}{2})F(0)$ (b) on the electron concentration n for different temperatures T ($g = 1$, $W = 0.2$, $h = 0.1$).

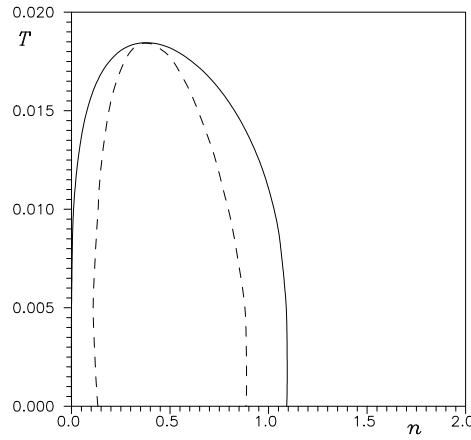


Fig. 7. Phase diagram ($T - n$) for phase separated state. Solid line: binodal, dashed line: spinodal ($g = 1$, $W = 0.2$, $h = 0.1$).

opposite case of $U = 0$. As a whole, such a picture of phase transitions into a new uniform phase is in agreement with the known results for the FK model in the case of strong coupling (see Ref. [43]). But, as is evident from the phase diagram obtained in Ref. [57] for this model, in the region of

large but finite values of g the phase with double modulation can appear. In order to detect instabilities associated with the wave vector $\mathbf{k} \neq \mathbf{0}$ one should calculate the susceptibility functions and analyse their temperature and \mathbf{k} -dependencies. Such an investigation was performed for PEM in the framework of GRPA (see below, Secs. 3.1.2 and 3.2.2).

3. Simplified PEM in Generalized Random Phase Approximation

A more complete investigation of the PEM was performed in the framework of the generalized random phase approximation (GRPA). Such an approach was formulated by Izyumov and Letfulov³⁹ for the calculation of the pair correlation functions and magnetic susceptibility of the Hubbard and $t - J$ models. It is based on the expansions in terms of electron transfer and consists in the summation of the diagrams having a structure of sequences of the electron loops (created by the electron Green's functions) joined by vertices of various types appearing due to short-range interactions.^{26,39}

Thermodynamics of PEM was studied in the GRPA for $U = 0$, $\Omega = 0$ (simplified model) in the cases of strong ($g \gg W$) and weak ($g < W$) coupling as well as in the limit of the infinitely large on-site electron repulsion ($U \rightarrow \infty$). Let us first consider the results obtained for simplified model.

3.1. Strong Coupling Case; $U = 0$, $\Omega = 0$

3.1.1. Thermodynamics of the Uniform State

First we consider the case of strong coupling. Here the single-site states can be used as the basic ones and the formalism of electron annihilation (creation) operators $a_{i\sigma} = b_{i\sigma} P_i^+$, $\tilde{a}_{i\sigma} = b_{i\sigma} P_i^-$ ($P_i^\pm = 1/2 \pm S_i^z$) acting at a site with certain pseudospin orientation was introduced.³⁰ Using this representation we can write the model Hamiltonian in the form

$$\begin{aligned} H &= H_0 + H_{\text{int}}, \\ H_0 &= \sum_i \{ \varepsilon(n_{i\uparrow} + n_{i\downarrow}) + \tilde{\varepsilon}(\tilde{n}_{i\uparrow} + \tilde{n}_{i\downarrow}) - h S_i^z \}, \\ H_{\text{int}} &= \sum_{ij\sigma} t_{ij} (a_{i\sigma}^+ a_{j\sigma} + a_{i\sigma}^+ \tilde{a}_{j\sigma} + \tilde{a}_{i\sigma}^+ a_{j\sigma} + \tilde{a}_{i\sigma}^+ \tilde{a}_{j\sigma}). \end{aligned} \quad (19)$$

Here, $\varepsilon = -\mu + g/2$ and $\tilde{\varepsilon} = -\mu - g/2$ are the energies of single-site states.

Expansion of the calculated quantities in terms of electron transfer leads to the infinite series of terms containing the averages of the T -products of

the $a_{i\sigma}$, $\tilde{a}_{i\sigma}$ operators. The evaluation of such averages is made using the corresponding Wick's theorem.^{30,58} The results are expressed in terms of the products of nonperturbed Green's functions and averages of a certain number of the projection operators P_i^\pm which are calculated by means of the semi-invariant expansion.³⁰

Nonperturbed electron Green's function is equal to

$$g(\omega_n) = \langle g_i(\omega_n) \rangle; \quad g_i(\omega_n) = \frac{P_i^+}{i\omega_n - \varepsilon} + \frac{P_i^-}{i\omega_n - \tilde{\varepsilon}}. \quad (20)$$

In the diagrammatic representation it has the meaning of the simplest irreducible Larkin part in the series for the free single-electron Green's function $G_{\mathbf{k}}(\omega_n)$. In the Hubbard-I type approximation (see previous section) $G_{\mathbf{k}}(\omega_n)$ can be written as a sum of the following chain diagrams

$$\text{---} \text{---} \text{---} = \text{---} \text{---} \text{---} + \text{---} \text{---} \text{---} + \dots, \quad (21)$$

or

$$G_{\mathbf{k}}(\omega_n) = [g^{-1}(\omega_n) - t_{\mathbf{k}}]^{-1}, \quad (22)$$

and its poles (after analytic continuation $i\omega_n \rightarrow \omega + i\delta$) determine the electron spectrum

$$\varepsilon_{I,II}(t_{\mathbf{k}}) = \frac{t_{\mathbf{k}}}{2} - \mu \pm \frac{1}{2} \sqrt{g^2 + 4t_{\mathbf{k}} \langle S^z \rangle g + t_{\mathbf{k}}^2}. \quad (23)$$

The electron subbands are divided by a gap which tends to zero only at $g \rightarrow 0$.

There are used here (and below) the following diagrammatic notations: $\bigcirc = S_i^z$, $\text{---} \text{---} \text{---} = g_i(\omega_n)$, wavy line is the electron intersite hopping t_{ij} . Semi-invariants are represented by ovals and contain the δ -symbols on the site indices.

In the adopted approximation the diagrammatic series for the pseudospin mean value can be presented in the form

$$\langle S^z \rangle = \bullet = \bigcirc - \text{---} \text{---} \text{---} + \frac{1}{2!} \text{---} \text{---} \text{---} - \dots \quad (24)$$

In the spirit of the traditional mean field approach⁵⁹ the renormalization of the basic semi-invariant by the insertion of independent loop fragments is taken into account in (24).

The analytical expression for the loop is as follows:

$$\begin{aligned} \text{Loop} &= \frac{2}{N} \sum_{n, \mathbf{k}} \frac{t_{\mathbf{k}}^2}{g^{-1}(\omega_n) - t_{\mathbf{k}}} \left(\frac{P_i^+}{i\omega_n - \varepsilon} + \frac{P_i^-}{i\omega_n - \tilde{\varepsilon}} \right) \\ &= \beta(\alpha_1 P_i^+ + \alpha_2 P_i^-). \end{aligned} \quad (25)$$

Similarly, the diagrammatic series for the electron concentration mean value is as follows:

$$\begin{aligned} \langle n_i \rangle &= \square - \text{Diagram 1} + \frac{1}{2!} \text{Diagram 2} - \dots \\ &+ \sum_{\alpha} \text{Diagram 3}, \end{aligned} \quad (26)$$

where $\square = n_i$, $\text{Diagram 1} = \frac{1}{i\omega_n - \varepsilon^{\alpha}}$, $\text{Diagram 2} = \frac{\langle P_i^{\alpha} \rangle}{i\omega_n - \varepsilon^{\alpha}}$, $\varepsilon^{\alpha} = (\varepsilon, \tilde{\varepsilon})$, $P_i^{\alpha} = (P_i^+, P_i^-)$.

The grand canonical potential Φ and pair correlation functions ($\langle S_i^z S_j^z \rangle$, $\langle S_i^z n_j \rangle$, $\langle n_i n_j \rangle$) are calculated according to self-consistent scheme of the GRPA: in sequences of loop diagrams in the expressions for Φ and correlators the connections between any two loops by more than one semi-invariant are omitted. We have, respectively

$$\begin{aligned} \Delta\Phi &= \frac{1}{2} \text{Diagram 1} + \frac{1}{3} \text{Diagram 2} + \dots \\ &+ \text{Diagram 3} - \frac{1}{2!} \text{Diagram 4} + \dots - \text{Diagram 5}. \end{aligned} \quad (27)$$

$$\begin{aligned} \langle S_i^z S_j^z \rangle &= \text{Diagram 1} = \text{Diagram 2} - \\ &- \sum_{\alpha, \beta} \text{Diagram 3}, \end{aligned} \quad (28)$$

$$\odot^\alpha = P_i^\alpha, \quad \text{---} \boxed{\alpha} \text{---} = \text{---} \triangleleft^\alpha \text{---} + \text{---} \triangleleft^\alpha \text{---} \text{---} \triangleleft^\alpha \text{---} \quad (29)$$

The first term in equation (28) takes into account a direct action of the internal effective self-consistent field on pseudospins:

$$\begin{aligned} \text{---} \odot^\alpha \text{---} &= \text{---} \odot^\alpha \text{---} - \text{---} \odot^\alpha \text{---} \text{---} \triangleleft^\alpha \text{---} + \\ &+ \frac{1}{2!} \text{---} \odot^\alpha \text{---} \text{---} \triangleleft^\alpha \text{---} \text{---} \triangleleft^\alpha \text{---} - \dots \end{aligned} \quad (30)$$

leading to the renormalization of the second-order semi-invariant due to the inclusion of “single-tail” loop-like parts. Second term in equation (28) describes an interaction between pseudospins which is mediated by electron hopping. From (24) and (25), the equation for the pseudospin mean value follows:

$$\langle S^z \rangle = \frac{1}{2} \tanh \left\{ \frac{\beta}{2} (h + \alpha_2 - \alpha_1) + \ln \frac{1 + e^{-\beta\varepsilon}}{1 + e^{-\beta\tilde{\varepsilon}}} \right\}, \quad (31)$$

where

$$\alpha_2 - \alpha_1 = \frac{2}{N} \sum_{\mathbf{k}} t_{\mathbf{k}} \frac{\varepsilon - \tilde{\varepsilon}}{\varepsilon_I(t_{\mathbf{k}}) - \varepsilon_{II}(t_{\mathbf{k}})} [n(\varepsilon_{II}(t_{\mathbf{k}})) - n(\varepsilon_I(t_{\mathbf{k}}))] . \quad (32)$$

The grand canonical potential in the considered approximation has the form:

$$\begin{aligned} \Delta\Phi = \Phi - \Phi|_{t=0} &= -\frac{2}{N\beta} \sum_{\mathbf{k}} \ln \frac{(\cosh \frac{\beta}{2} \varepsilon_I(t_{\mathbf{k}})) (\cosh \frac{\beta}{2} \varepsilon_{II}(t_{\mathbf{k}}))}{(\cosh \frac{\beta}{2} \varepsilon) (\cosh \frac{\beta}{2} \tilde{\varepsilon})} \\ &+ \langle S^z \rangle (\alpha_2 - \alpha_1) - \frac{1}{\beta} \ln \cosh \left\{ \frac{\beta}{2} (h + \alpha_2 - \alpha_1) + \ln \frac{1 + e^{-\beta\varepsilon}}{1 + e^{-\beta\tilde{\varepsilon}}} \right\} \\ &+ \frac{1}{\beta} \ln \cosh \left\{ \frac{\beta}{2} h + \ln \frac{1 + e^{-\beta\varepsilon}}{1 + e^{-\beta\tilde{\varepsilon}}} \right\}. \end{aligned}$$

With respect to the initial GRPA scheme,^{26,39} the action of the internal effective self-consistent field on pseudospins is taken into account by including the mean field type contributions into the expressions for all thermodynamic quantities. The electron concentration and pseudospin mean values as well as correlation functions are calculated consistently with the thermodynamics functions. It can be checked explicitly^{30,31} using the relations

$$\frac{d\Phi}{d(-\mu)} = \langle n \rangle; \quad \frac{d\Phi}{d(-h)} = \langle S^z \rangle; \quad \frac{dS^z}{d(-\beta h)} = \langle S^z S^z \rangle_{q=0}. \quad (33)$$

At high temperatures, equation (31) possesses only a uniform solution $\langle S_i^z \rangle = \langle S^z \rangle$. However, there exists a possibility of phase transition between different uniform phases with the different pseudospin mean values. For the first time the possibility of such a transition, which leads to the structural (dielectric) instability, was considered for the PEM in the limit of the strong electron correlation ($U \rightarrow \infty$) in Refs. [25,26] (this issue is analysed below, see Sec. 4). A relatively complete description of this transition was also given in Ref. [60] for the PEM with a direct interaction between pseudospins (in the $t_{ij} = 0$ limit).

Within the GRPA scheme presented here, the uniform-uniform phase transition in the simplified PEM was analysed in Ref. [30]. The solutions of the set of equations (33) which correspond to the absolute minimum values of $\Delta\Phi$ were determined and analysed. The calculations were numerically performed for the square lattice with the nearest-neighbour hopping ($d = 2$ DOS with the bandwidth $2W$). The obtained picture of the phase transition in the $\mu = \text{const}$ and $n = \text{const}$ regimes is very similar to the case of DMFT approach. When the chemical potential is fixed, there exist jumps of the pseudospin mean value and electron concentration on the phase transition line (Fig. 8). The $(h - \mu)$ and $(T_c - h)$ phase diagrams are nearly the same by their shape as in the DMFT case despite the fact that electron energy spectrum in GRPA is split at any values of g , see Fig. 9, 10. The same conclusion can be made when we compare the $(T - n)$ phase diagrams obtained in the $n = \text{const}$ regime; the corresponding phase separation areas are shown in Fig. 11. The difference in positions of critical points in the (h, T) plane calculated in the DMFT and GRPA approaches is also small (see Figs. 4 and 10b).

In figures discussed above, the case is presented when the chemical potential is placed in the lower energy subband. If μ is placed in the upper subband, the results are transformed according to the internal symmetry of the Hamiltonian and the following replacements should be made

$$\mu \rightarrow -\mu, \quad h \rightarrow 2g - h, \quad n \rightarrow 2 - n, \quad S^z \rightarrow -S^z. \quad (34)$$

Summing up, we can conclude that the generalization of GRPA scheme,^{30,31} which takes into account the mean-field loop-like contributions to the semi-invariant averages, makes it possible to calculate the thermodynamic functions and to investigate the first order phase transitions between different uniform phases. At the transitions, there always remains a gap (in the strong coupling case, $g \gg W$) in the electron spectrum. With the change of the mean value of the pseudospin a reconstruction of the elec-

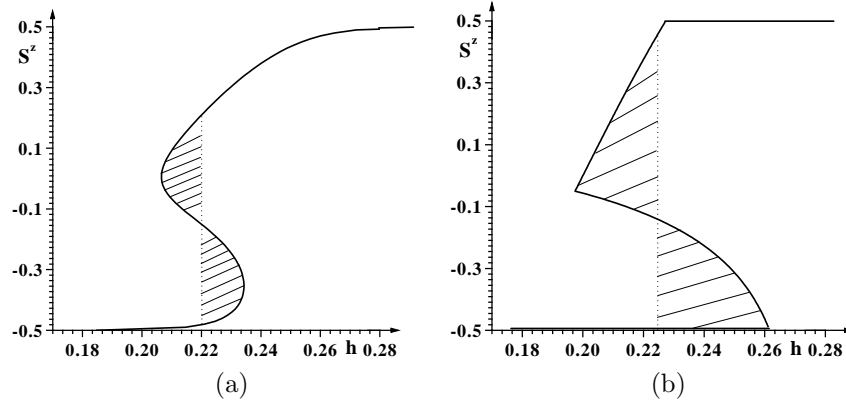


Fig. 8. Field dependence of $\langle S^z \rangle$ ($W = 0.2$, $\mu = -0.4$, $g = 1.0$) for $\mu = \text{const}$ regime; $T = 0.01$ and $T = 0$.

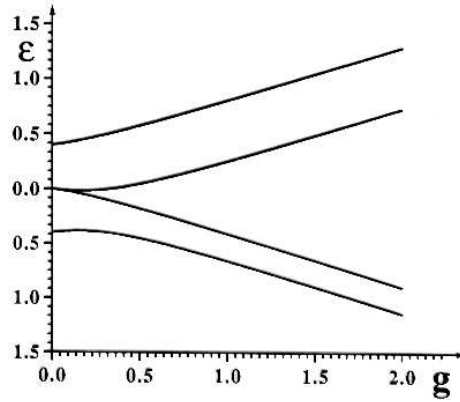


Fig. 9. Electron bands boundaries ($t_0 = 0.4$, $\langle S^z \rangle = 0.2$).

tron spectrum takes place, at which the widths of the electron subbands change which results in the jump-like change of electron concentration (at the given chemical potential μ , it corresponds to a charge transfer from /to the electron reservoir).

The phase coexistence curve in the (h, T) plane is tilted from the vertical line; therefore, there is a possibility of the first order phase transition with the temperature change (in the narrow interval of the field h values). It

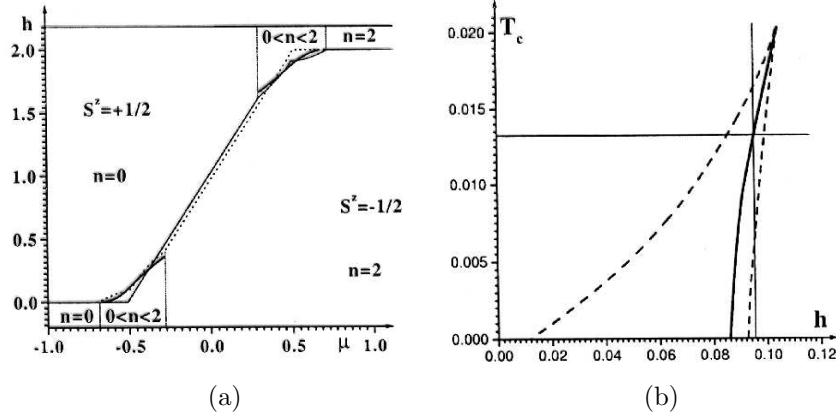


Fig. 10. (a): $(h - \mu)$ phase diagram ($T = 0$, $t_0 = 0.2$, $g = 1$). (b): $(T_c - h)$ phase diagram ($g = 1$, $t_0 = 0.2$, $\mu = -0.5$).

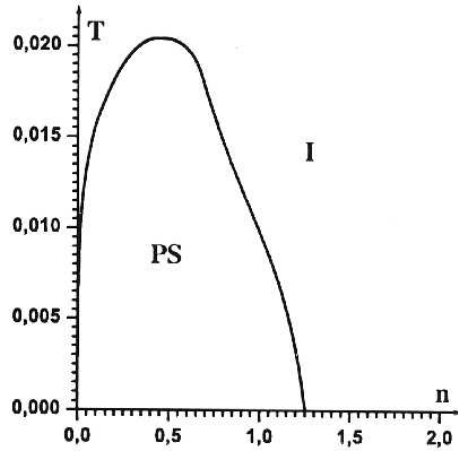


Fig. 11. $(T - n)$ phase diagram ($h = 0.1$, $t_{k=0} = 0.2$, $g = 1$).

should be noted that the existence of the shifted and tilted coexistence curve (as the result of the local pseudospin-electron interaction) was obtained for the first time in Ref. [60] for a PEM with the direct interaction between pseudospins. In the case considered here, such a direct interaction is not included, but due to electron transfer there appears an indirect one (the

latter is formed by the loop-like contributions $\Pi_{\mathbf{q}}$. The relative role of the direct and indirect interactions between pseudospins is analysed more in detail in Sec. 5, on the example of the two-sublattice PEM.

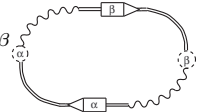
Herein below, considering the $\langle S^z S^z \rangle$ pair correlation function, we shall look at the possibility of the spatially modulated charge (charge density wave, CDW) and pseudospin orderings in the PEM with $U = 0$, $\Omega = 0$ in the strong coupling case.

3.1.2. The Chess-Board Phase

The analysis of the $\langle S^z S^z \rangle_{\mathbf{q}}$ correlator temperature behaviour shows that for certain values of model parameters, the high temperature phase may be unstable with respect to fluctuations with $\mathbf{q} \neq \mathbf{0}$.³¹ Solution of Eq. (28) for pseudospin correlator has the form

$$\langle S^z S^z \rangle_{\mathbf{q}} = \frac{1/4 - \langle S^z \rangle^2}{1 + \Pi_{\mathbf{q}}(\frac{1}{4} - \langle S^z \rangle^2)}, \quad (35)$$

where $\Pi_{\mathbf{q}}$ characterizes an interaction between pseudospins via electron subsystem:

$$\Pi_{\mathbf{q}} = \sum_{\alpha, \beta} (-1)^{\alpha+\beta} \langle \alpha | \langle \beta | \text{ (diagram) } | \beta \rangle | \alpha \rangle, \quad (36)$$


and its singularities

$$1 + \Pi_{\mathbf{q}}(\frac{1}{4} - \langle S^z \rangle^2) = 0$$

give the instability points of uniform phase.

It follows from calculations³¹ that for some model parameter values, the uniform phase becomes unstable with respect to fluctuations with $\mathbf{q} = (\pi, \pi)$ (the chess-board phase).

To consider the thermodynamics of the chess-board phase analytically, we take into account the modulation of the pseudospin and electron distribution, introducing two kinds of sites: $\langle S_1^z \rangle$ and n_1 correspond to one sublattice and $\langle S_2^z \rangle$ and n_2 to the other one. In this case the single-electron Green's function for the l sublattice is equal to:

$$G_l(\mathbf{k}, \omega_n) = \frac{g_l(\omega_n)}{1 - t_{\mathbf{k}}^2 g_1(\omega_n) g_2(\omega_n)}, \quad (37)$$

where $g_l(\omega_n)$ ($l = 1, 2$) is the nonperturbated Green's function for sublattice l . The single-electron spectrum is determined from the equation

$$x^4 - (g^2/2 + t_{\mathbf{k}}^2)x^2 - gt_{\mathbf{k}}^2(\langle S_1^z \rangle + \langle S_2^z \rangle)x + g^4/16 - g^2 t_{\mathbf{k}}^2 \langle S_1^z \rangle \langle S_2^z \rangle = 0. \quad (38)$$

The roots $\varepsilon_1(t_{\mathbf{k}}) \geq \varepsilon_2(t_{\mathbf{k}}) \geq \varepsilon_3(t_{\mathbf{k}}) \geq \varepsilon_4(t_{\mathbf{k}})$ of the equation (38) form four subbands. The widths of subbands depend on the mean values of pseudospins.

The branches $\varepsilon_1(t_{\mathbf{k}})$, $\varepsilon_2(t_{\mathbf{k}})$, on the one side, and $\varepsilon_3(t_{\mathbf{k}})$, $\varepsilon_4(t_{\mathbf{k}})$ on the other side, form two pairs of bands which are always separated by a gap. The equation for pseudospin mean values (31) can be now written in the form:

$$\langle S_l^z \rangle = \frac{1}{2} \tanh \left\{ \frac{\beta}{2} (h + \alpha_2^l - \alpha_1^l) + \ln \frac{1 + e^{-\beta\varepsilon}}{1 + e^{-\beta\tilde{\varepsilon}}} \right\}, \quad l = 1, 2 \quad (39)$$

where expressions for the effective self-consistent fields are

$$\alpha_2^l - \alpha_1^l = \frac{2}{N} \sum_{\mathbf{k}} t_{\mathbf{k}}^2 (\varepsilon - \tilde{\varepsilon}) \sum_{i=1}^4 A_i^l n[\varepsilon_i(t_{\mathbf{k}}) - \mu], \quad (40)$$

$$A_i^l = \frac{\varepsilon_i(t_{\mathbf{k}}) + g \langle S_l^z \rangle}{(\varepsilon_i(t_{\mathbf{k}}) - \varepsilon_j(t_{\mathbf{k}}))(\varepsilon_i(t_{\mathbf{k}}) - \varepsilon_p(t_{\mathbf{k}}))(\varepsilon_i(t_{\mathbf{k}}) - \varepsilon_m(t_{\mathbf{k}}))}, \quad i \neq j, p, m, \quad l \neq l'.$$

Expression for the electron mean number follows from (33):

$$\begin{aligned} \langle n_1 + n_2 \rangle &= \frac{2}{N} \sum_{\mathbf{k}} \sum_{i=1}^4 n[\varepsilon_i(t_{\mathbf{k}}) - \mu] \\ &- 2 \left[(\langle P_1^+ \rangle + \langle P_2^+ \rangle) n(\tilde{\varepsilon}) + (\langle P_1^- \rangle + \langle P_2^- \rangle) n(\varepsilon) \right], \end{aligned} \quad (41)$$

and the grand canonical potential (27) can be written for the two-sublattice case in the following analytic form:

$$\begin{aligned} \Delta\Phi &= -\frac{2}{N\beta} \sum_{\mathbf{k}} \ln \frac{\prod_{i=1}^4 \cosh \left[\frac{\beta}{2} (\varepsilon_i(t_{\mathbf{k}}) - \mu) \right]}{(\cosh \frac{\beta}{2} \varepsilon)^2 (\cosh \frac{\beta}{2} \tilde{\varepsilon})^2} + \sum_{l=1,2} \langle S_l^z \rangle (\alpha_2^l - \alpha_1^l) \\ &+ \sum_{l=1,2} \left[-\frac{1}{\beta} \ln \cosh \left\{ \frac{\beta}{2} (h + \alpha_2^l - \alpha_1^l) + \ln \frac{1 + e^{-\beta\varepsilon}}{1 + e^{-\beta\tilde{\varepsilon}}} \right\} \right. \\ &\left. + \frac{1}{\beta} \ln \cosh \left\{ \frac{\beta}{2} h + \ln \frac{1 + e^{-\beta\varepsilon}}{1 + e^{-\beta\tilde{\varepsilon}}} \right\} \right]. \end{aligned} \quad (42)$$

As previously in the investigation of equilibrium conditions, we consider two different thermodynamic regimes.

a) The $\mu = \text{const}$ regime.

The equilibrium is defined by the minimum condition of Φ (42). Numerical analysis of solutions of equations (39)-(41) which satisfy this criterion,

was performed in Ref. [31]. The examples of the calculated field dependencies of $\langle S_1^z - S_2^z \rangle$ (the order parameter for the chess-board phase) and grand canonical potential are presented in Fig. 12 for low temperatures (the case $g \gg W$ is considered). It is seen from comparison of the Φ values for the uniform and the chess-board phases that the modulated phase is thermodynamically stable at intermediate values of the h field in the region between points a and b . These points correspond to the first and second order phase

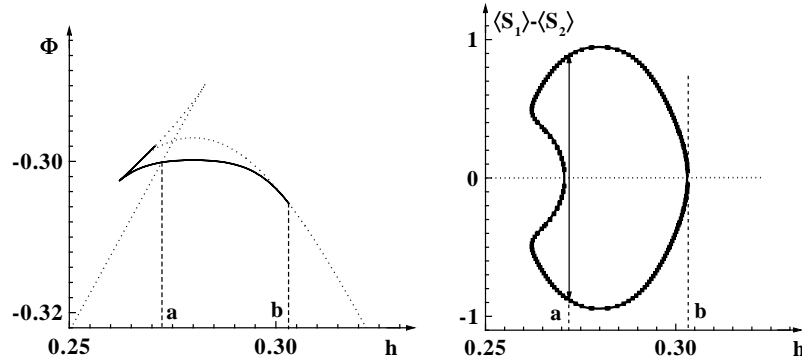


Fig. 12. Field dependence of the grand canonical potential and order parameter ($T = 0.005$, $\mu = -0.36$, $W = 0.2$, $g = 1$). Dotted and solid lines correspond to the uniform and the chess-board phases, respectively. See the text for a whole description.

transitions, respectively. In the first case, the jump-like change of order parameter is accompanied by characteristically similar changes of the subband widths and, as a result, by changes of the electron concentration.

The resulting phase diagram ($h - \mu$) at low temperatures is shown in Fig. 13. The chess-board phase exists as an intermediate phase between the uniform phases with different $\langle S^z \rangle$ and n values. Transitions between the uniform and modulated phases are of the first or second order and can be realized in the case when μ is placed in ε_2 or ε_3 subbands or between them. Transitions between different uniform phases (described in the previous section), which are of the first order, take place when the chemical potential is placed within the ε_1 , ε_4 and partially within ε_2 , ε_3 subbands.

The shape of the $(T - h)$ phase diagram strongly depends on the μ value. In the case when μ is placed in the ε_3 subband, such a diagram is shown in Fig. 14a. With the temperature increase, the first order phase transition between the uniform and the chess-board phases transforms into the first order phase transition between uniform phases and, finally, disappears in

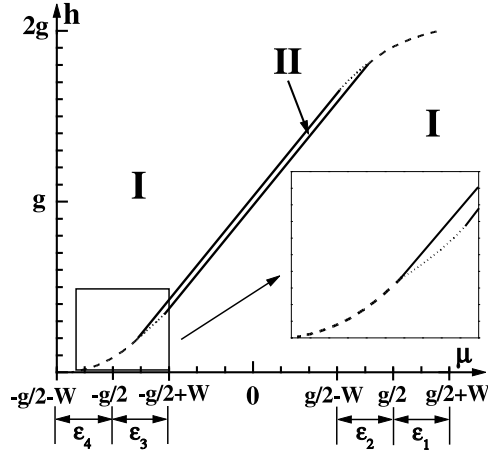


Fig. 13. $(h-\mu)$ phase diagram ($T = 0.005$, $W = 0.2$, $g = 1$). I: uniform phase, II: chess-board phase. Dashed lines: first order phase transitions between the uniform phases with different pseudospin mean values. Dotted lines: first order phase transitions between the uniform and the chess-board phases. Solid lines: second order phase transitions.

the critical point θ_c . The diagram shows the possibility of the first order phase transitions between uniform phases and either first or second order ones between the uniform and the chess-board phases at the change of temperature.

In the case when chemical potential lies between the ε_1 , ε_2 and ε_3 , ε_4 subbands, the transitions between phases I (uniform) and II (chess-board) are of the second order; the corresponding $(T-h)$ diagram is shown in Fig. 14b.

b) The $n = \text{const}$ regime.

In this regime, the equilibrium is defined by a minimum of the free energy $F = \Phi + \mu N$. This condition forms a set of equations (39) and (41) for the pseudospin mean values and chemical potential. The obtained dependencies of F and μ on the electron concentration are presented in Fig. 15.

One can see the regions with $d\mu/dn \leq 0$ where the phase separation into regions with different phases (the uniform and the chess-board phases in this case) and with different electron concentrations and pseudospin mean values take place.

Based on the obtained results, the phase diagram $(n-h)$ was constructed (Fig. 16). The phase separation into regions with the uniform and the chess-

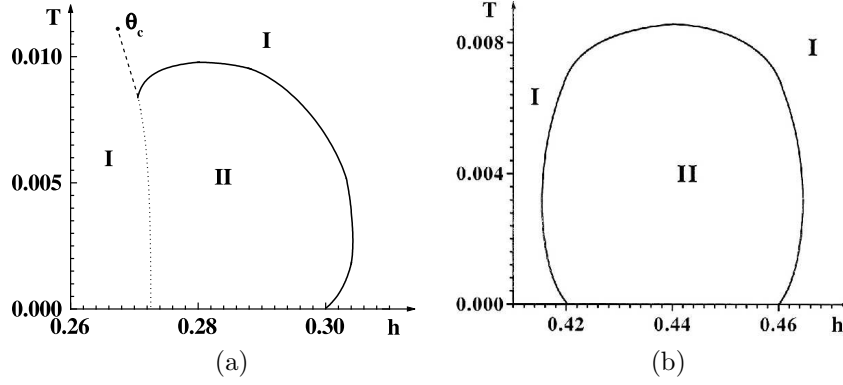


Fig. 14. (a): Phase diagram ($T-h$) ($\mu = -0.36$, $W = 0.2$, $g = 1$). I: uniform phase, II: chess-board phase. Dashed lines: first order phase transitions between different uniform phases (bistability). Dotted line: first order phase transitions between the uniform and the chess-board phases. Solid lines: second order phase transitions. (b): Phase diagram ($T-h$) ($\mu = -0.28$, $t_{k=0} = 0.2$, $g = 1$).

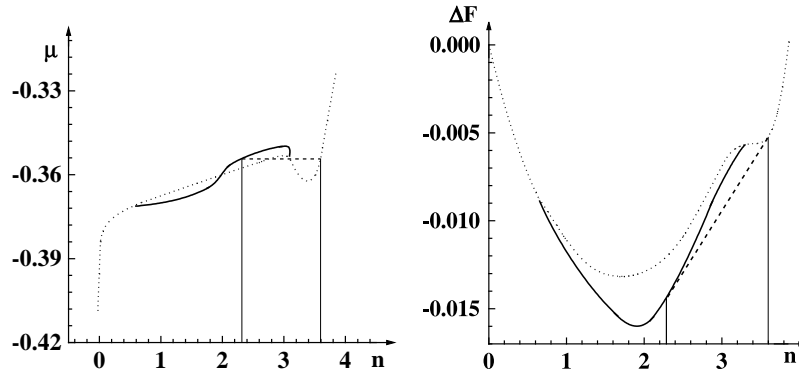


Fig. 15. Dependence of the chemical potential μ on the electron concentration n and deviation of the free energy from linear dependence ($T = 0.005$, $h = 0.28$, $W = 0.2$, $g = 1$). Dashed line: phase separation area. Dotted line: uniform phase. Solid line: chess-board phase.

board phases takes place when the chemical potential is placed within the subbands ε_2 , ε_3 . That agrees with the results obtained in the $\mu = \text{const}$ case when within this area we had the first order phase transition between the corresponding phases.

The phase separated and the chess-board phase regions narrow with

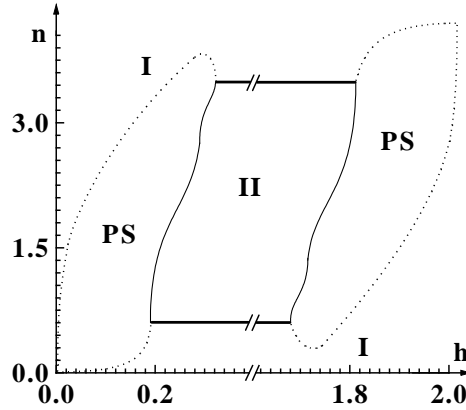


Fig. 16. Phase diagram ($n - h$) ($T = 0.005$, $W = 0.2$, $g = 1$). I: uniform phase, II: chess-board phase, PS: phase separation area.

the temperature increase, but thick solid lines in Fig. 16 approach faster one another and, for high enough temperatures, we have only the phase separation into the regions with uniform phases.

The fact of the existence of doubly-modulated (chess-board) phase in the PEM as intermediate one between segregated phases (at low temperatures) is similar to the results obtained in DMFT for the Falicov-Kimball model by Freericks and Lemansky.⁶¹ Investigation of temperature T_c of instability of the high-temperature phase of the FK model as a function of the ordering wave vector (determined by the divergence of the relevant susceptibility) showed that near half-filling ($\rho_e = 0.5$) the chess-board phase is stable, while the segregated phase exists at the occupations near electron band edges. The region of modulated phase narrows at the increase of g and disappears at $g \rightarrow \infty$.⁵⁷ In this limit the thermodynamically stable states were analyzed⁶² based on the calculations of the grand canonical potential and the phase separation diagrams (where besides the spinodal lines the lines of the first order transition temperatures were shown) were built; the cases of different electron concentrations ρ_e were considered.

Nevertheless, one cannot claim the one-to-one correspondence. The calculations of Freericks and Lemansky were performed in another thermodynamic regime: the concentration of heavy particles ρ_i was fixed (that would correspond to the given value of $\langle S^z \rangle$ for PEM). The closest to our case are the results obtained by Brandt and Mielsch.⁶³ They constructed the $(T - \rho_i)$ diagrams at the finite g values for the FK model. The obtained

sequence of phases (segregated-modulated-segregated) when ρ_i increases (from $\rho_i = 0$ up to $\rho_i = 1$) is the same as for PEM at the increase of the field h .

3.2. Weak Coupling Case; $U = 0$

Now let us consider the case of weak coupling ($g < W$). We can base on the perturbation theory approach taking the mean field Hamiltonian as the zero-order one.³² We use the approximation

$$gn_i S_i^z \rightarrow gn_i \langle S_i^z \rangle + g \langle n_i \rangle S_i^z - g \langle n_i \rangle \langle S_i^z \rangle \quad (43)$$

in this case, based on the arguments that for the simplified PEM with $U = 0$ the interaction constant g plays the role which is similar to that of U in the Hubbard model, and at the decrease of g below the critical value ($g \sim W$) the system should pass to the mean field regime of the Hartree-Fock type.

Having in mind the possibility that the system can be in the uniform or modulated state, we shall consider, as above, two different cases. The first one corresponds to the homogeneous pseudospin ordering and spatially uniform mean distribution of electrons. The second one is the case of modulation with doubling of the lattice period (chess-board phase).

3.2.1. Uniform Phase

The Hamiltonian of PEM in the mean-field approximation (MFA) reads

$$H = H_{el} + H_s + U, \quad (44)$$

$$H_{el} = \sum_{i,\sigma} (g\eta - \mu) n_{i,\sigma} + \sum_{i,j,\sigma} t_{i,j} a_{i,\sigma}^+ a_{j,\sigma},$$

$$H_s = \sum_i [(gn - h) S_i^z + \Omega S_i^x], \quad (45)$$

$$U = -g \sum_i n\eta = -Ngn\eta.$$

The parameters $\langle n_i \rangle = n$ and $\langle S_i^z \rangle = \eta$ are determined from the set of equations

$$n = \frac{1}{N} \sum_{\mathbf{k}\sigma} (e^{\beta(g\eta + t_{\mathbf{k}} - \mu)} + 1)^{-1} \equiv \frac{1}{N} \sum_{\mathbf{k}\sigma} f(g\eta + t_{\mathbf{k}}), \quad (46)$$

$$\eta = \frac{h - gn}{2\lambda} \tanh\left(\frac{\beta\lambda}{2}\right); \quad \lambda = \sqrt{(gn - h)^2 + \Omega^2}.$$

The grand canonical potential in the MFA is given by the expression

$$\frac{\Phi}{N} = -\frac{T}{N} \sum_{\mathbf{k}, \sigma} \ln(1 + e^{\frac{\mu - t_{\mathbf{k}} - g\eta}{T}}) - T \ln(2 \cosh \frac{\beta\lambda}{2}) - gn\eta \quad (47)$$

where $\lambda = \sqrt{(gn - h)^2 + \Omega^2}$.

Similarly to the strong coupling case, we can distinguish the regimes of the constant electron chemical potential $\mu = \text{const}$ (where the stable states can be found from the minimum Φ condition) and the given electron concentration $n = \text{const}$ (when one should find the minimum of the free energy $F = \mu n + \Phi$).

a) Thermodynamics in the $\mu = \text{const}$ regime.

We consider at first the simplest case $\mu = 0$, $h = g$. Here the solution $\eta = 0$, $n = 1$ of the set of equations (46) exists at any temperature and describes a disordered phase. Furthermore, at low temperatures there appears a non-zero solution $\eta \neq 0$, $n \neq 1$. A critical temperature T_c is determined from the equation

$$1 + \frac{g^2}{2\Omega} \tanh \frac{\beta\Omega}{2} \Pi_0 = 0, \quad (48)$$

which in the case $\Omega \rightarrow 0$ reduces to the form

$$1 + \frac{\beta}{4} g^2 \Pi_0 = 0, \quad (49)$$

Here

$$\Pi_0 = \frac{2}{N} \sum_{\mathbf{k}} f'(t_{\mathbf{k}}) = 2 \int_{-W}^W dt \rho(t) f'(t). \quad (50)$$

In the low temperature limit we have $T_c = \frac{g^2}{2} \rho(0)$ (when the DOS at the Fermi level $\rho(\mu)|_{\mu=0}$ is finite). In the case $\Omega \neq 0$ there exists such a critical value $\Omega_{cr} = g^2 \rho(0)$ ($\Omega_{cr} = \frac{g^2}{2W}$ for the rectangular DOS), above which (at $\Omega > \Omega_{cr}$) the phase transition to ordered phase disappears. This is equivalent to the existence of a critical value of g : at given Ω the phase transition is possible when $g > g_{cr} = \sqrt{\frac{\Omega}{\rho(0)}}$. In the case of the DOS with logarithmic singularity, the critical temperature exists at any values of the tunneling splitting parameter Ω and at $\frac{\Omega}{g} \gg \frac{g}{W}$ we have an asymptotic expression:

$$T_c \approx 2eW \exp\left(\frac{-\Omega W \pi^2}{2g^2}\right). \quad (51)$$

The physical nature of the phase transition considered here at $h = g$, $\mu = 0$ (the fixed μ regime) is as follows: the appearance of an ordered phase is

connected with its stabilization due to the shift of the electron band down to the low energy values under the effect of the internal field; this ensures the corresponding gain in the electron energy (it should be mentioned that the electron band spectrum in this case remains unsplit in the uniform phase; only the shift of the band as a whole can take place).

This mechanism remains the main reason of the phase transition when the initial electron band is not half-filled. In this case (when $\mu \neq 0$) we performed the investigation using the numerical calculations when the set of equations (46) is solved and using the expression (47) for the grand canonical potential Φ . The selection of solutions was carried out using the condition of the absolute minimum of Φ .

As can be seen,³² below T_c the system undergoes the first order phase transition with jumps of the mean values of the electron concentration and pseudospin at the change of the field h ; the phase transition point is determined using the Maxwell rule. The similar transition takes place at the change of the chemical potential at fixed h . The presence of the tunneling-like splitting decreases the temperature of the phase transition at the fixed values of μ and h .

The regions of coexistence of phases with different values of the electron concentration and pseudospin are shown in the plane (μ, h) at $\Omega = 0$ and $\Omega \neq 0$ in Figs. 17.

Phase transition lines in the plane (T, h) at different values of μ are shown in Fig. 18. Such a line is vertical for the case $\mu = 0$ only; for the case $\mu \neq 0$, the line is bent. This makes the first order phase transition possible at the change of temperature (with the jumps of the parameters η, n). The slopes of the phase equilibrium curves are opposite for $\mu > 0$ and $\mu < 0$. The lines of the critical points are shown for the cases $\Omega = 0, \Omega \neq 0$; the calculations are carried out using rectangular density of states. Similar phase diagrams are obtained using direct momentum summation for square lattice (Fig. 19). As in the case of rectangular DOS, the maximum T_c is achieved at $\mu = 0$ but the critical temperature line has a more pronounced peak.

b) Thermodynamics in the $n = \text{const}$ regime.

The values n_1, n_2 and η_1, η_2 between which the jumps of the electron concentration and pseudospin mean value take place at the phase transitions in the $\mu = \text{const}$ case, correspond to the phases which coexist in the phase transition points. In the regime $n = \text{const}$, there is a phase separation on the phases with the above mentioned values of n and μ . For example, at the parameter value $\Omega = 0, h = 0.7, T = 0.008$, the

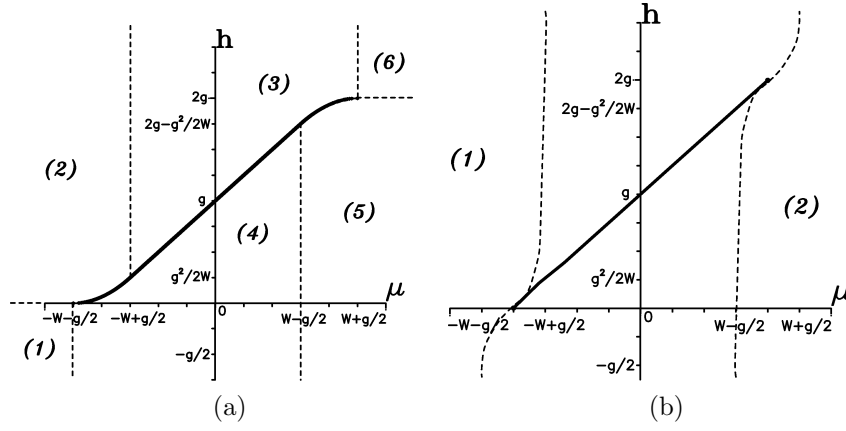


Fig. 17. (a): The ground state diagram ($T = 0, \Omega = 0$). Regions with different n, η values are separated by dashed lines and a solid line (the phase transition line): (1) $n = 0, \eta = -1/2$; (2) $n = 0, \eta = 1/2$; (3) $\eta = 1/2, n = 1 + \frac{\mu}{W} - \frac{g}{2W}$; (4) $\eta = -1/2, n = 1 + \frac{\mu}{W} + \frac{g}{2W}$; (5) $n = 2, \eta = -1/2$; (6) $n = 2, \eta = 1/2$. (b): The $(h - \mu)$ phase diagram ($T = 0.004, \Omega = 0.12$). Regions with different n, η values are separated by dashed lines and a solid line (the phase transition line): (1) $n \approx 0, \eta \approx \frac{1}{2} \frac{h}{\sqrt{h^2 + \Omega^2}}$; (2) $n \approx 2, \eta \approx \frac{1}{2} \frac{h-2g}{\sqrt{(h-2g)^2 + \Omega^2}}$.

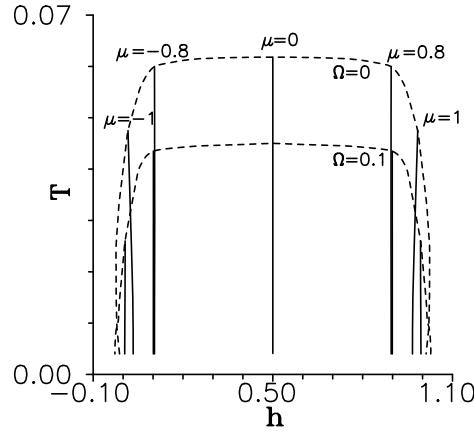


Fig. 18. The critical temperature lines (dashed lines) and the phase transition lines (solid lines) for $\Omega = 0$ and $\Omega = 0.1$ (the case of the rectangular DOS).

system is unstable with respect to the phase separation in the region $n_1 = 1.149 < n < n_2 = 1.645$.³²

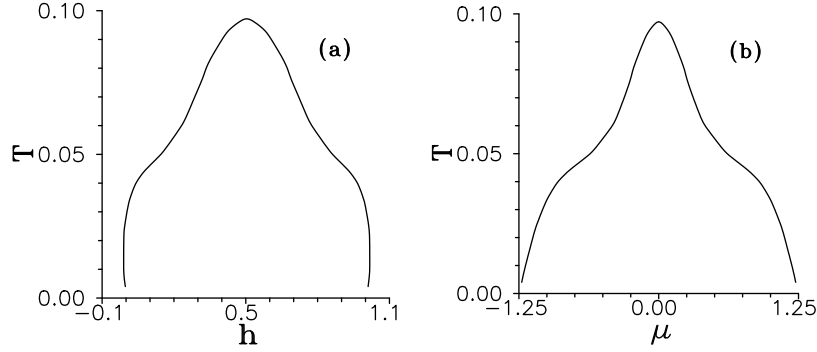


Fig. 19. The critical temperature lines on the a) (h, T) and b) (μ, T) planes for $\Omega = 0$ (direct momentum summation is used).

Phase separation regions are shown in Fig. 20 at different temperatures (the calculations were carried out for square lattice using direct momentum summation when solving the set of equations (46)). At the increase of temperature the separation region narrows and at $T > T_c$ it disappears. The presence of the tunneling-like splitting leads to the decrease of the area of phase separation region and to the lowering of T_c .

It can be noted that at weak coupling, when only uniform states are considered, we have one phase separation region in the (h, n) plane while in the strong coupling case ($g \gg W$) there exist two such regions at the distance of order g along h axis; the modulated phase is placed between

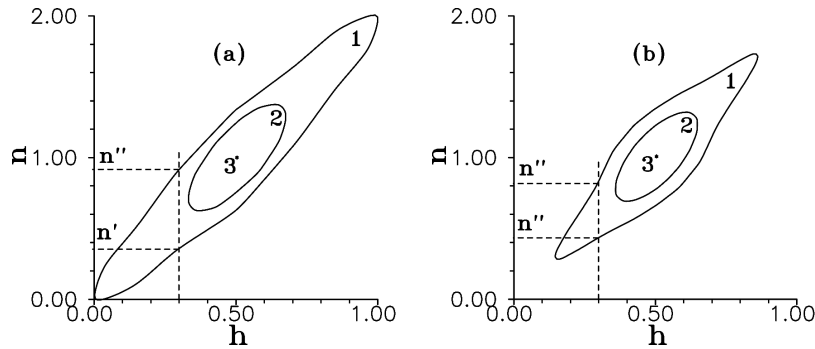


Fig. 20. $(n - h)$ -phase diagram in the cases a) $\Omega = 0$; b) $\Omega = 0.1$. Phase separation regions for different temperatures are shown. a) 1: $T = 0.008$, 2: $T = 0.08$, 3: $T = 0.0972$; b) 1: $T = 0.008$, 2: $T = 0.075$, 3: $T = 0.0903$.

them³¹ (see also Sec. 3.1.2).

3.2.2. Phase with Double Modulation

Let us consider now the thermodynamics of the simplified PEM in the case of doubly modulated phase. The possibility for such a phase was shown at a strong coupling ($g \gg W$); the necessary condition was the location of the chemical potential between the split electron subbands. Now (at $g < W$) the band is unsplit and in such a situation there must be another mechanism of stabilizing the lattice modulation.

At the double modulation the crystal can be divided into two sublattices ($\alpha = 1, 2$), and the parameters $\eta_\alpha = \langle S_{i\alpha}^z \rangle$, $n_\alpha = \sum_\sigma \langle n_{i\alpha\sigma} \rangle$ can be introduced (i is an unit cell index). Similarly to the homogeneous phase, the mean field approximation is used. The modulation leads to the splitting in the electron spectrum due to difference between the internal field acting in sublattices

$$\lambda_{\mathbf{k}\alpha} = g \frac{\eta_1 + \eta_2}{2} + (-1)^\alpha \sqrt{(g \frac{\eta_1 - \eta_2}{2})^2 + t_{\mathbf{k}}^2} \quad (52)$$

(the similar effect takes place in the FK model⁶⁴). The initial band is divided into two subbands separated by the gap $\Delta = g|\eta_1 - \eta_2|$ (see Fig. 21).

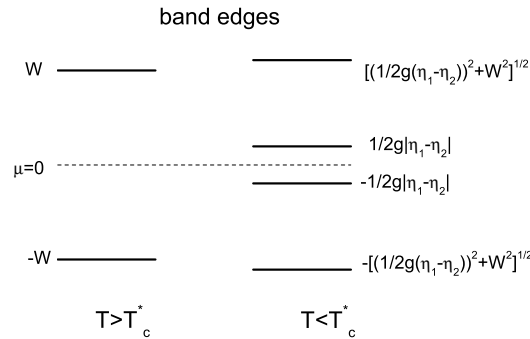


Fig. 21. The band edges for the cases $T > T_c^*$ (homogeneous phase) and $T < T_c^*$ (the double modulation case); $\mu = 0$, $h = g$.

Contributions from both sublattices are present in the equation for the

electron concentration in sublattices

$$n_\alpha = \frac{1}{N} \sum_{\mathbf{k}\sigma} \left(\frac{1 + \cos 2\phi}{2} (e^{\beta(\lambda_{\mathbf{k}\alpha} - \mu)} + 1)^{-1} + \frac{1 - \cos 2\phi}{2} (e^{\beta(\lambda_{\mathbf{k}\beta} - \mu)} + 1)^{-1} \right), \quad (53)$$

where

$$\cos 2\phi = \frac{-g \frac{\eta_1 - \eta_2}{2}}{\sqrt{(g \frac{\eta_1 - \eta_2}{2})^2 + t_{\mathbf{k}}^2}}$$

can be obtained diagonalizing the mean-field two-sublattice Hamiltonian of the model.³² Another equation which appears as a result of the averaging of the operator $S_{i\alpha}^z$ has the form

$$\eta_\alpha = \frac{h - gn_\alpha}{2\tilde{\lambda}_\alpha} \tanh\left(\frac{\beta\tilde{\lambda}_\alpha}{2}\right). \quad (54)$$

Here

$$\tilde{\lambda}_\alpha = \sqrt{(gn_\alpha - h)^2 + \Omega^2}. \quad (55)$$

In the mean field approximation, the grand canonical potential for the double modulation case has the form

$$\begin{aligned} \frac{2\Phi}{N} = & -\frac{T}{N} \sum_{\mathbf{k}, \sigma} \ln((1 + e^{-\frac{\lambda_{\mathbf{k}1} - \mu}{T}})(1 + e^{-\frac{\lambda_{\mathbf{k}2} - \mu}{T}})) \\ & -T \ln(4 \cosh \frac{\beta\tilde{\lambda}_1}{2} \cosh \frac{\beta\tilde{\lambda}_2}{2}) - g(n_1\eta_1 + n_2\eta_2). \end{aligned} \quad (56)$$

The solution of the set of equations for the n_α and η_α parameters and the investigations of thermodynamically stable states were carried out numerically.³² It was established that phase transitions from the uniform to the low temperature modulated phase are of the second or first order. This is illustrated in Fig. 22, where the phase transition lines at $\mu = 0$ are shown for $\Omega = 0$ and $\Omega \neq 0$ (here a direct momentum summation is used in calculations); the tricritical points are also present here.

The difference $\delta n = n_1 - n_2$ (as well as the difference $\delta \eta = \eta_1 - \eta_2$) can play a role of the order parameter for the modulated phase. Coming from the equations for δn and $\delta \eta$ we obtain the following condition of the appearance of nonzero solutions

$$\begin{aligned} 1 = & \frac{g}{N} \sum_{\mathbf{k}\sigma} \frac{1}{t_{\mathbf{k}}} \left(e^{\beta(g\eta - t_{\mathbf{k}} - \mu)} + 1 \right)^{-1} \\ & \times \left[\beta g \frac{(h - gn)^2}{\lambda^2} \left(\frac{1}{4} - \langle \sigma^z \rangle^2 \right) + g \langle \sigma^z \rangle \frac{\Omega^2}{\lambda^3} \right]. \end{aligned} \quad (57)$$

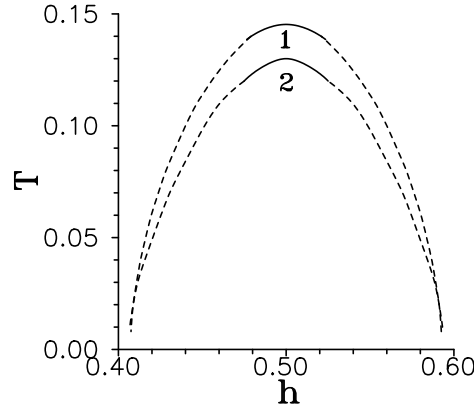


Fig. 22. The phase transition lines (solid and dashed lines are the lines of the second and of the first order phase transitions, respectively) from the uniform phase to the phase with double modulation (1 : $\Omega = 0$; 2 : $\Omega = 0.2$).

Proceeding from this equation, we can find a critical temperature T_c^* as the maximum temperature (among the set of temperatures which are obtained for different h values) which fulfills this equation at a fixed value of the chemical potential. This temperature is the point of the second order phase transition to modulated phase at the corresponding value of the field h .

In the symmetric case, when $\mu = 0$, $h = g$ and in the high-temperature phase $n = 1$, $\eta = 0$, the equation (57) reduces to the form

$$1 = -\frac{g^2}{\Omega} \tanh \frac{\beta\Omega}{2} \frac{1}{N} \sum_{\mathbf{k}} \frac{1}{t_{\mathbf{k}}} f(t_{\mathbf{k}}). \quad (58)$$

The critical temperatures T_c^* , obtained in the cases of rectangular DOS and DOS with logarithmic singularity, are, respectively,

$$T_c^* \approx \frac{eW}{2} \exp \left(-\frac{2\Omega W}{g^2} \right) \quad (59)$$

and

$$T_c^* \approx 2eW \exp \left(-\frac{\pi\sqrt{\Omega W}}{g} \right). \quad (60)$$

In both cases, they are higher than the corresponding temperatures T_c for transitions between uniform phases and remain finite at high Ω values.

It can be seen that $T_c^* > T_c$ also at $\mu \neq 0$, but for the μ values, which are less than the certain ($|\mu| < \mu_0$) value. The typical dependencies of T_c^*

and T_c on μ are shown in Fig. 23 in the cases $\Omega = 0$ and $\Omega \neq 0$. One can conclude that in the case of the electron band occupation close to the half-filling, the transition to modulated phase should be realized. The transition between two different uniform phases is possible only when μ is placed near the band edges.

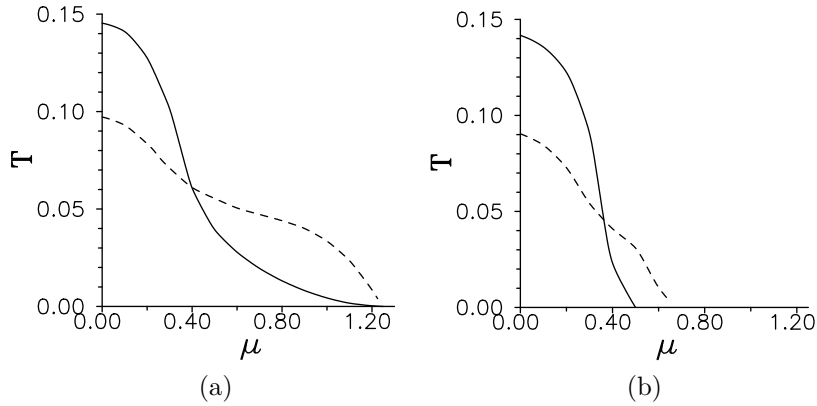


Fig. 23. The dependence of the critical temperature on the chemical potential; a) $\Omega = 0$ b) $\Omega = 0.1$. Solid line refers to the case of the phase with double modulation, dashed line refers to the transition into the homogeneous phase.

An existence of the first order phase transitions between uniform and doubly modulated phases, shows the possibility of a separation into these two phases. This takes place at certain values of the electron concentration. The corresponding $(n - h)$ diagrams are shown in Fig. 24. The borders of the separation regions were obtained from the convexity condition of the free energy defined as $F/N = \Phi/N + n\mu$. As temperature increases, the separation area narrows, but in the middle of it there appears a region of the chess-board phase existence. This is an additional feature which supplements the picture of separation shown in Fig. 20. At high enough temperatures, only the second order phase transition into the doubly modulated state remains and the phase separation region disappears.

3.2.3. Pair Correlation Function and Susceptibilities

The analysis of thermodynamically stable equilibrium states of the PEM in the case of weak coupling can be supplemented by an investigation of temperature and wave vector dependencies of the pseudospin, electron density

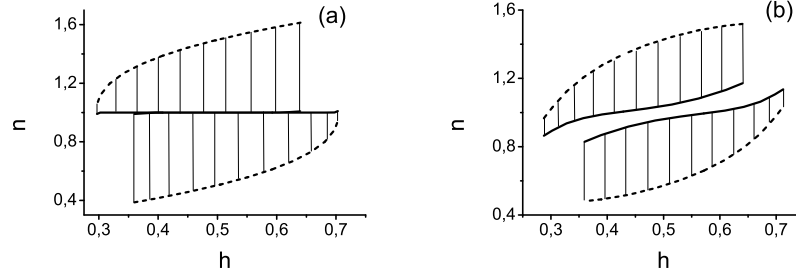


Fig. 24. $(n-h)$ phase diagram, $\Omega = 0$. Phase separation regions are shown for different temperatures: a) $T = 0.008$, b) $T = 0.08$. Dashed lines denote the borders of the uniform phase, thick solid lines denote the borders of the phase with doubly modulated lattice period.

and mixed pair correlation function. The corresponding Green's functions were calculated in Ref. [33] within the GRPA scheme. The cases of isothermal response were considered, where the isothermal susceptibility

$$\chi_T(\mathbf{q}, \omega_n) = \int_0^\beta \langle T_\tau M(0) M(\tau) \rangle_{\mathbf{q}} e^{i\omega_n \tau} d\tau - \beta \langle M \rangle^2 \delta(\omega_n) \quad (61)$$

is expressed in terms of the Matsubara Green's function and the so-called "isolated" response, which is described by means of the two-time Zubarev Green's function

$$\chi_I(\mathbf{q}, \omega) \sim \langle \langle M | M \rangle \rangle_{\mathbf{q}\omega}. \quad (62)$$

The dipole moment M_i of the unit cell was taken in the form: $M_i = d_e n_i + d_s S_i^z$; here the electron contribution due to nonhomeopolarity of occupancy of the electron orbitals was taken into account besides the pseudospin contribution.

Such an expression for dipole moment comes from the form of transverse component of polarization in the case of the YBaCuO structure. The electron component corresponds to the charge transfer in a perpendicular direction from/to the Cu_2O_2 layers (with the participation of the Cu-O chains), while the pseudospin component is connected with the redistribution of the ionic charges when O_4 ion moves from one equilibrium position to another.^{26,65}

Similarly to the above considered strong coupling case, the simple sequences of loop diagrams are taken into account in the diagrammatic representation for Matsubara's correlators. The connections between loops

are accomplished by semi-invariants or by the boson (pseudospin) Green's functions. The contribution that corresponds to the separate link is (see Ref. [33])

$$\Sigma_{\mathbf{q}}(\omega) = \frac{1}{2} \sin^2 \vartheta [K_{\mathbf{q}}^0(\omega_n) + K_{\mathbf{q}}^0(-\omega_n)] \langle \sigma^z \rangle_0 - M_{\mathbf{q}}(\omega_n). \quad (63)$$

Here

$$K_{\mathbf{q}}^0(\omega_n) = \frac{1}{i\omega_n - \lambda}; \quad M_{\mathbf{q}}(\omega_n) = \beta b' \cos^2 \vartheta \delta(\omega_n),$$

$$\sin \vartheta = \Omega/\lambda; \quad \langle \sigma^z \rangle_0 = b = \frac{1}{2} \tanh \frac{\beta \lambda}{2}; \quad b' = \frac{\partial b}{\partial(\beta \lambda)}. \quad (64)$$

The pseudospin Green's function $K_{\mathbf{q}}^0(\omega_n)$ is constructed of operators of the transverse pseudospin components acting in the rotated reference system ($K_{\mathbf{q}}^0 \sim \langle T \sigma^+ \sigma^- \rangle$; $\sigma_i^z = S_i^z \cos \vartheta - S_i^x \sin \vartheta$; $\sigma_i^x = S_i^x \cos \vartheta + S_i^z \sin \vartheta$) and has a pole at λ (the pseudospin reversal energy). The semi-invariant $M_{\mathbf{q}}(\omega_n)$, describing the correlation of longitudinal pseudospin components ($\sim T \langle \sigma^z \sigma^z \rangle^c$), is proportional to $\delta(\omega)$. There is no such contribution in $\Sigma_{\mathbf{q}}(\omega)$ when the Green's functions are calculated using the equation of motion and the decoupling procedure for Zubarev's functions. Thus, the isothermal (χ_T) and isolated (χ_I) susceptibilities do not coincide for PEM.³³ It should be mentioned that a similar result is also obtained in the cases $U \rightarrow \infty$ ²⁶ and $t_{ij} \rightarrow 0$.²⁵

In the GRPA scheme, the summation of loop sequences leads to the expression for pseudospin correlator

$$\langle T S^z S^z \rangle_{\mathbf{q}, \omega} = - \frac{\Sigma_{\mathbf{q}}(\omega)}{1 - g^2 \Sigma_{\mathbf{q}}(\omega) \Pi_{\mathbf{q}}(\omega)}, \quad (65)$$

where

$$\Pi_{\mathbf{q}}(\omega) = \frac{2}{N} \sum_{\mathbf{k}} \frac{n(t_{\mathbf{k}}) - n(t_{\mathbf{k}-\mathbf{q}})}{\omega + t_{\mathbf{k}} - t_{\mathbf{k}-\mathbf{q}}} \quad (66)$$

is the standard electron loop contribution.

The condition $\langle T S^z S^z \rangle_{\mathbf{q}, \omega=0} \rightarrow \infty$ (which corresponds to divergence of isothermal susceptibility χ_T) indicates an instability with respect to transition into modulated (at $q \neq 0$) or another uniform (at $q = 0$) phase. The thermodynamic parameter values, at which $\chi_T \rightarrow \infty$, determine the spinodal points.

The equation

$$\lambda^2 + g^2 \sin^2 \vartheta \lambda \langle \sigma^z \rangle_0 \Pi_{\mathbf{q}} + \lambda^2 g^2 \beta b' \cos^2 \vartheta \Pi_{\mathbf{q}} = 0 \quad (67)$$

was solved together with equation (46) for the mean values η and n written in MFA. The function $\Pi_{\mathbf{q}}$ was calculated numerically by the direct momentum summation for square lattice.

At fixed values of chemical potential, the critical point can be defined as an upper point of spinodal (on the (T, h) plane) with the highest temperature depending on the wave vector \mathbf{q} value. Fig. 25 shows the dependencies of the critical temperature and the corresponding wave vector on the chemical potential in the case $\Omega = 0$ (only positive values of the chemical potential are shown; at $h = g$, the picture is symmetrical with respect to the point $\mu = 0$ which coincides with the centre of the energy band). We can see that the case $\mathbf{q} = (\pi, \pi)$ is realized when $|\mu| \lesssim 0.25$ at chosen parameter values, which means that the system can pass into the phase with doubly modulated lattice period. The case $\mathbf{q} = 0$ (transition into the uniform phase) is realized when $0.85 \lesssim |\mu| \leq 1.25$.^a The system undergoes transition to the incommensurate phase at intermediate values of the chemical potential. The presence of tunneling splitting narrows the interval of values of μ at which the above mentioned transitions take place; at high enough values of Ω , the transition into the chess-board phase occurs only.

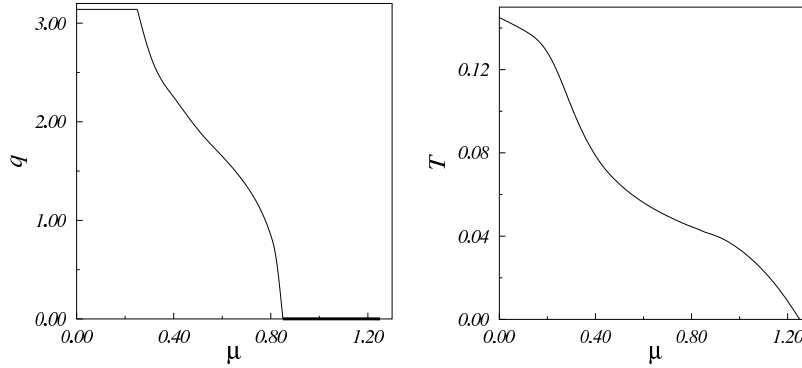


Fig. 25. The dependence of the modulation wave vector $\mathbf{q}=(q,q)$ and the temperature of absolute instability of high-temperature phase on the chemical potential, $\Omega = 0$, $g = 0.5$.

The given results at $\Omega = 0$ generally correspond to the picture of phase transitions in the FK model obtained in DMFT in the case of weak coupling.^{57,63,66} It was shown for FK model that at small values of n the

^a1.25 = $W + g/2$; this value corresponds to the upper edge of the band when $\langle S^z \rangle = \frac{1}{2}$.

phase separation can be realized, while near half-filling of the band the chess-board phase is preferable and, finally, at intermediate values of n the appearance of phase with an incommensurate modulation is possible. The transitions into one or another phase were observed by the divergences of corresponding susceptibilities. It should be mentioned that such a procedure did not enable the authors to reveal the thermodynamically stable states in the regions where the instabilities of the both types (at $\mathbf{q} = 0$ and $\mathbf{q} = (\pi/a, \pi/a, \dots)$) are superimposed; this problem can be solved based on the analysis of the behaviour of the grand canonical potential.

The GRPA scheme used here to investigate the PEM is advantageous in interpreting the dielectric susceptibility divergences due to the explicit dependence of the $\chi_T(\mathbf{q}, 0)$ function on the wave vector. In the DMFT approach at $d \rightarrow \infty$ such a dependence enters only through the function $X(\mathbf{q}) = \frac{1}{d} \sum_{j=1}^d \cos q_j$ that leads to some difficulties in considering the incommensurate ordering. Besides, in Refs. [57, 63, 66] there was used a regime of a fixed concentration of localized particles; in the PEM this corresponds to the regime $\langle S^z \rangle = \text{const}$. In this case, the authors came to a conclusion that the transition to the chess-board phase at $g < W$ is always continuous and spinodals are the lines of phase transitions.⁶¹ In such a situation the separation into the uniform and modulated phases would be impossible. Contrary to that, by analysing the behaviour of the grand canonical potential we showed that the transition to the chess-board phase can be both of the second order (the spinodals are the phase transition lines) and of the first order (spinodals do not coincide with phase transition lines). Due to the first order phase transition to the chess-board phase, the possibility of the phase separation into the uniform and the chess-board phases in the case of weak coupling was demonstrated. Such a possibility, as was shown in Ref. [64], see also Sec. 3.1.2, exists in the case of large values of coupling constant. It should be mentioned that in Ref. [61] only the possibility of phase separation into different uniform phases was investigated.

Though the phase transitions in the PEM at weak coupling are similar to the transitions revealed in this model in the case of strong interaction, $g \gg W$,^{30,31} the physical mechanisms of transitions are to a greater extent distinct. In the case of strong coupling, the electron spectrum is always split due to the one-site interaction. The mechanism which ensures the advantage of the transition is connected with the different character of the electron spectrum reconstruction in the subbands and with the corresponding redistribution of the electron density of states. At weak coupling, a new phase,

which appears at the transition between uniform phases, is stabilized due to the shift of the electron band as a whole. The phase with a double modulation appears due to energy gain at the splitting of the initial band at the Fermi level (the effect is similar to the Peierls instability at the interaction with phonons). Besides that, the dependencies of the critical temperatures on the coupling constant g are different in the both cases: T_c (or T_c^*) is proportional to g^2 at $g \ll W$, while at $g \gg W$ the critical temperatures decrease ($\sim \frac{1}{g}$) when g increases (such a type of behaviour of T_c^* for the FK model was obtained in Refs. [51, 63]).

3.3. Superconductivity in the PEM

Due to the presence of intrinsic dynamics, the PEM at $\Omega \neq 0$ also possesses an instability with respect to transition into superconducting (SC) state. Under certain conditions the transition to SC state will compete with the transition to modulated phase (CDW). Among others, close attention to this problem for an electron system interacting with anharmonic structure units was paid in Ref. [67]. It was shown that, when there is no electron correlation, the transition temperature to CDW, T_p , is higher than that to SC, T_c . The authors, however, considered only the case where the local potential is symmetric and the electron filling is close to a half. The question concerning the appearance of superconductivity for a wider range of the model parameters and electron concentrations has not been examined. It was just the point of investigation performed in Ref. [34] within the GRPA. To examine the possibility of the appearance of SC phase we calculated the static susceptibility χ^{SC} in the superconducting channel. Taking into account the diagrams which correspond to ladder approximation (with the parallel directions of lines of the fermion Green's functions), we obtained the Bethe-Salpeter equation for the superconducting vertex part $\Gamma_{\omega_1, \omega_2}(\mathbf{k}_1, \mathbf{k}_2)$ ³⁴

$$\Gamma = \Gamma^0 + T \sum_{\mathbf{k}_3, \omega_3} \Gamma^0 \chi^0 \Gamma, \quad (68)$$

where $\chi_{\omega_1}^0(\mathbf{k}_1) = \frac{1}{N} G_{\mathbf{k}_1}^0(\omega_1) G_{-\mathbf{k}_1}^0(-\omega_1)$; $\Gamma^0 = g^2 \langle T S^z S^z \rangle_{\mathbf{k}_2 - \mathbf{k}_1, \omega_1 - \omega_2}$ is given by the expression (65). The susceptibility

$$\chi^{SC} = \frac{1}{N} \sum_{\mathbf{k}, \mathbf{q}} \int_0^\beta \langle T_\tau a_{\downarrow \mathbf{k}}(\tau) a_{\uparrow - \mathbf{k}}(\tau) a_{\uparrow - \mathbf{q}}^+ a_{\downarrow \mathbf{q}}^+ \rangle e^{i\omega_n \tau} d\tau \quad (69)$$

is connected with the vertex part Γ in the following way

$$\frac{1}{T}\chi^{SC} = \sum_{\omega, \mathbf{k}} \chi_{\omega}^0(\mathbf{k}) + T \sum_{\mathbf{k}_1, \mathbf{k}_2, \omega_1, \omega_2} \chi_{\omega_1}^0(\mathbf{k}_1) \Gamma_{\omega_1, \omega_2}(\mathbf{k}_1, \mathbf{k}_2) \chi_{\omega_2}^0(\mathbf{k}_2). \quad (70)$$

Both approximations, the ladder one for the $\Gamma_{\omega_1, \omega_2}(\mathbf{k}_1, \mathbf{k}_2)$ vertex construction and the chain (GRPA) one for the construction of $\Gamma_{\omega_1, \omega_2}^0(\mathbf{k}_1, \mathbf{k}_2)$, were employed by analogy with what was done in the $t - J$ model for the SC description.⁶⁸ The mentioned approximations correspond to the known Migdal-Eliashberg (ME) one, which is usually used in considering the electron-phonon systems, particularly in the Holstein model. Considering the phonon frequencies to be small in comparison with the transfer integral,⁶⁹ one gets results in qualitative agreement with the quantum Monte Carlo simulations.²² Since the PEM is similar to the Holstein model, and may be considered as a double-level approximation of the latter one, the ME approximation is expected to be satisfactory in the limits of non-half filling, low temperatures, and small Ω .

A way to find the SC transition temperature is to determine a temperature, at which the susceptibility in the superconducting channel diverges. It corresponds to the condition when the scattering matrix

$$T_{\omega_1 \omega_2}(\mathbf{k}_1, \mathbf{k}_2) = T \chi_{\omega_1}^0(\mathbf{k}_1) \Gamma_{\omega_1 \omega_2}^0(\mathbf{k}_1, \mathbf{k}_2) \quad (71)$$

has an eigenvalue which is equal to unity.^{69,70} In calculations performed in Ref. [34], the approximation $\Gamma^0 \approx -g^2 \Sigma$, similar to the non-renormalized ME approximation in the Holstein model,⁶⁹ was used. This can be done in the high-temperature phase, when the system has not still passed to the CDW state. In such a case the unperturbed vertex part does not depend on the wave vector and thus the unit eigenvalue of the matrix

$$\tilde{T}_{\omega_1 \omega_2} = T \sum_{\mathbf{k}_1} \chi_{\omega_2}^0(\mathbf{k}_1) \Gamma_{\omega_1 \omega_2}^0 \quad (72)$$

should be found at first. Of all the temperatures within the (T, h) plane which satisfy this condition, the highest one is chosen as the critical SC transition temperature.

Numerical calculations performed in Ref. [34] show that the SC transition in the simplified PEM is possible (in the weak coupling case) at the electron concentrations away from half-filling (when the chemical potential is placed near the electron band edges) and outside the region of the above described transitions with the modulation of the electron and pseudospin density (see Fig. 26). Such a picture is similar to that obtained

within the DMFT for the Holstein model⁶⁹ (but, in the latter case, the incommensurate phase does not appear at the intermediate values of μ). This is also consistent with the results obtained by quantum Monte-Carlo simulations.^{22,71} These papers just established that SC could appear at low temperatures; the transition to incommensurate CDW was not studied.

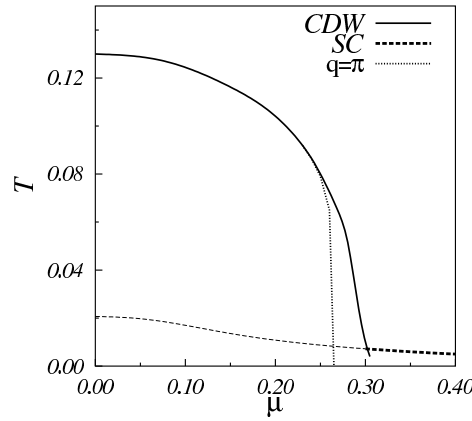


Fig. 26. The temperature of the absolute instability of the high-temperature phase with respect to the transitions to CDW (solid line) and SC (bold dashed line) as functions of the chemical potential, for $\Omega = 0.2$ and $g = 0.5$. Dotted line shows the temperature of the transition to the phase with the modulation wave vector $\mathbf{q} = (\pi, \pi)$.

The estimates performed in Ref. [34] show that at $W \approx 0.5$ eV and $g \approx 0.25$ eV, the maximum value of the SC transition temperature is $T_{max}^{SC} \approx 10 - 40$ K. This agrees with the conclusions obtained for PEM in Ref. [67], where calculations were performed by analogy with the scheme used for the Eliashberg equations in the limit of a weak electron-phonon interaction, provided that the renormalization of the pseudospin excitation energy is neglected. According to the estimations carried out in Ref. [72], if there were no CDW, the SC transition temperature would be $T^{SC} \approx 40$ K at the band filling close to a half.

The question of what occurs in the systems as the tunneling splitting frequency grows further is also of great interest. It was shown in Ref. [32] that, at $\mu = 0$, the critical temperature of transition to the phase with double lattice period modulation, T_c^{CDW} , decreases with the increase in Ω according to the exponential law: $T_c^{CDW} \sim \exp\left(-\frac{\pi\sqrt{\Omega W}}{g}\right)$, see (60). It

follows from the analysis of the behaviour of the $\tilde{T}_{\omega_1\omega_2}$ matrix elements³⁴ that the SC transition temperature, T_c^{SC} , changes with Ω in a similar way. In this case, for $\mu = 0$, $T_c^{\text{SC}} (\Omega \rightarrow \infty) \approx T_c^{\text{CDW}} (\Omega \rightarrow \infty)$. As is seen from Fig. 26, with the increase in $|\mu|$, the CDW transition temperature falls more rapidly than the SC one. Thus, for the non-zero values of the chemical potential, provided that Ω is sufficiently large, the SC transition temperature is expected to be higher than the CDW one, and there will only be the transition to SC. However, as was noted above, to make the correct analysis of the competition between these transitions, the renormalized Γ^0 vertex should be used when solving Eq. (71) and determining T_{SC} . Moreover, when Ω values are sufficiently large, the applicability of the approximation in deriving this equation turns out to be unjustified.

The mechanism that leads in the PEM to SC, which we have considered here, as well as the traditional phonon one, does not result in high values of T_c , and apparently it does not explain the HTSC phenomenon.

4. Thermodynamics of PEM at Finite U Values; the $U \rightarrow \infty$ Limit

The analysis similar to the one given above was performed in Refs. [24–26, 73–76] for the PEM with $U \neq 0$. The presence of the electron-electron on-site interaction leads to some differences in the behaviour of the model with respect to the case of FK model (even if $\Omega = 0$). The consideration was based on expansions in terms of electron transfer t_{ij} , as in the strong coupling limit $g \gg W$.

The single-site Hamiltonian

$$H_i = U n_{i\uparrow} n_{i\downarrow} - \mu (n_{i\uparrow} + n_{i\downarrow}) + g (n_{i\uparrow} + n_{i\downarrow}) S_i^z - h S_i^z - \Omega S_i^x \quad (73)$$

that includes the U -term can be reduced to the diagonal form using the rotation transformation $|R\rangle = \alpha_{Rr}^{(\varphi_r)} |r\rangle$,^{26,73} where $|R\rangle = |n_{i\uparrow}, n_{i\downarrow}, S_i^z\rangle$ is the single-site basis of states

$$\begin{aligned} |1\rangle &= |0, 0, 1/2\rangle & |\tilde{1}\rangle &= |0, 0, -1/2\rangle \\ |2\rangle &= |1, 1, 1/2\rangle & |\tilde{2}\rangle &= |1, 1, -1/2\rangle \\ |3\rangle &= |0, 1, 1/2\rangle & |\tilde{3}\rangle &= |0, 1, -1/2\rangle \\ |4\rangle &= |1, 0, 1/2\rangle & |\tilde{4}\rangle &= |1, 0, -1/2\rangle, \end{aligned} \quad (74)$$

and

$$\cos \varphi_r = \frac{n_r g - h}{\sqrt{(n_r g - h)^2 + \Omega^2}}. \quad (75)$$

In terms of Hubbard operators $X^{rs} = |r\rangle\langle s|$, acting on the new basis, the transformed Hamiltonian of the model is

$$H = \sum_{ir} \lambda_r X_i^{rr} + \sum_{ij\sigma} t_{ij} a_{i\sigma}^+ a_{j\sigma} \quad (76)$$

with

$$\lambda_{ri\tilde{r}} = U\delta_{r,r} + E_0 n_r \pm \frac{1}{2} \sqrt{(n_r g - h)^2 + \Omega^2}$$

and

$$a_{i\sigma}^+ = \sum_{mn} A_{mn}^\sigma X_i^{mn}, \quad a_{i\sigma} = \sum_{mn} A_{mn}^\sigma X_i^{nm}. \quad (77)$$

Here $n_1 = 0$, $n_2 = 2$, $n_3 = n_4 = 1$ ($n_{\tilde{r}} = n_r$); expressions for A_{mn}^σ are given in Ref. [26].

The detailed consideration of single-electron spectrum of model (1) at $U \neq 0$ was performed in Refs. [23, 74] in the Hubbard-I approximation. The interaction with the anharmonic (pseudospin) mode splits the energy levels of ordinary Hubbard model 0, E_0 and $2E_0 + U$ into sublevels $\lambda_{r,\tilde{r}}$. As a result, each Hubbard single-electron band splits into four subbands. In the independent subband approximation

$$\varepsilon_{rs}(\mathbf{q}) = \lambda_r - \lambda_s + t_{\mathbf{q}} (A_{rs}^\sigma)^2 \langle X^{rr} + X^{ss} \rangle, \quad (78)$$

where $(rs) = (41), (\tilde{4}\tilde{1}), (\tilde{4}\tilde{1}), (4\tilde{1}), (23), (\tilde{2}\tilde{3}), (\tilde{2}\tilde{3}), (2\tilde{3})$ for $\sigma = \uparrow$ and substitution $4 \leftrightarrow 3$ should be done for $\sigma = \downarrow$. The widths and statistical weights of the subbands are determined by parameters A_{rs}^σ . The four lower and four higher bands correspond to the hole and electron pair motion, respectively. Their positions depend on the value of the asymmetry field h (see Fig. 27, where the band edges as functions of h are shown at the fixed value of μ).

Thermodynamics and dielectric properties of PEM with $U \neq 0$ were studied in Refs. [26, 75]. Being interested in the problem of lattice instabilities in high- T_c superconductors of YBaCuO - type we calculated the transverse dielectric susceptibility (corresponding to the ε_{zz} component for YBaCuO - structure), using, as above (see Sec. 3.2.3), the expression $P_i = d_s S_i^z + d_e n_i$ for local dipole moment. We can respectively separate ion, electron and mixed components in the total susceptibility

$$\begin{aligned} \chi_\perp(\mathbf{q}, \omega_n) &= d_s^2 \chi^{SS}(\mathbf{q}, \omega_n) + d_e^2 \chi^{nn}(\mathbf{q}, \omega_n) \\ &+ d_s d_e (\chi^{Sn}(\mathbf{q}, \omega_n) + \chi^{nS}(\mathbf{q}, \omega_n)), \end{aligned} \quad (79)$$

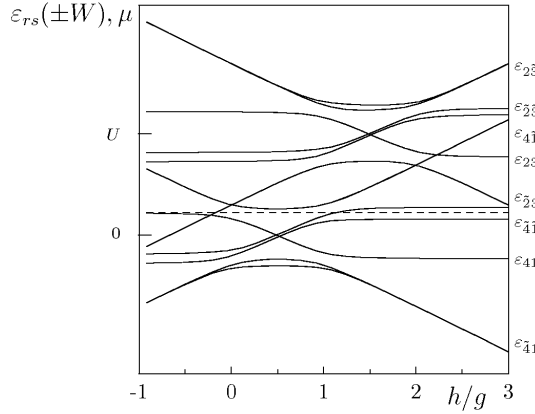


Fig. 27. Single-electron spectrum depending on h/g in the $\mu = \text{const}$ regime; $U = 2.2$, $g = 1$, $h = 0.7$, $\Omega = 0.3$, $W = 0.2$, $\mu = 0.5$.

where $\chi^{AA'} = K^{AA'}$ in the regime $\mu = \text{const}$ (when we fix the value of the chemical potential and permit the charge redistribution between conducting sheets Cu_2O_2 and other structural elements, having in mind an application of the model to the YBaCuO-type crystals) and

$$\chi^{AA'} = K^{AA'} - \frac{K^{An} K^{nA'}}{K^{nn}} \quad (80)$$

in the regime $n = \text{const}$ (when we fix the electron concentration n in the conducting sheets Cu_2O_2).²⁶ Here $K^{AA'}(\mathbf{q}, \omega_n)$ are Fourier-transforms of semi-invariant Matsubara's Green's functions

$$K_{lm}^{AA'}(\tau - \tau') = \langle T \tilde{A}(\tau) \tilde{A}'_m(\tau') \rangle^c \quad (81)$$

constructed of the operators S_i^z , n_i .

In the case of zero hopping ($t_{ij} = 0$) the exact expressions for correlation functions $\chi^{ss}(\omega_n)$, $\chi^{nn}(\omega_n)$, $\chi^{ns}(\omega_n)$ can be easily obtained.²⁵

For $n = \text{const}$ regime the main contribution into susceptibility is produced by the pseudospin subsystem. The susceptibility

$$X^{ss} \cong \frac{ds^r}{vc} \sum_{r=1}^4 \frac{\Omega^2}{[(n_r g - h)^2 + \Omega^2]^{3/2}} \langle X^{\tilde{r}\tilde{r}} - X^{rr} \rangle \quad (82)$$

as a function of h generally possesses three peaks. The maxima at $h = 0$, g and $2g$ correspond to the points of possible dielectric instabilities (that can appear due to the proximity of corresponding energy subbands). The intensities of peaks are redistributed with the change of n ; this is illustrated in Fig. 28a for the case $U/W \gg 1$ ($\Omega = 0.3g$, $0 < n < 1$), when only two peaks are present; the first peak disappears at $n \rightarrow 1$ and the second one disappears at $n \rightarrow 0$. The effect remains the same at $t_{ij} \rightarrow 0$.

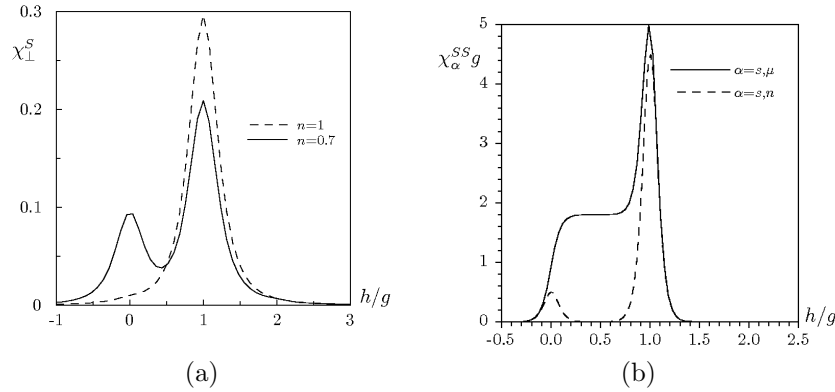


Fig. 28. (a): Dielectric susceptibility as a function of h/g at different electron concentrations; $U = 2.2$, $g = 1$, $h = 0.7$, $\Omega = 0.3$, $W = 0.2$, $d_S = 0.6$. (b): Pseudospin component of susceptibility $\chi_\alpha^{SS}g$ vs h/g for $\Omega = 0$ ($\omega_n = 0$, $n = 0.9$, $T/g = 0.05$).

In the $\mu = \text{const}$ regime there are three regions of h values ($h < 0$, $0 < h < g$ and $h > g$) with different field and temperature behaviour of susceptibility (see Fig. 28b). This is a result of the difference in the direction and value of the total effective field $h - n_i g$ acting on the pseudospin at site i when electron occupation on this site changes ($n_i = 0$ or 1), which testifies to a strong correlation between electron and pseudospin subsystem.

The behaviour of transverse dielectric susceptibility χ^{ss} as a function of the field h and temperature becomes more complicated when we take into account the electron transfer. The calculations of components of susceptibility (79) were performed^{25,26} at $t_{ij} \neq 0$ in the particular case of no tunneling splitting in anharmonic potential well ($\Omega = 0$).

Green's functions (81), constructed of the operators

$$n_{i\sigma} = \sum_{r=1}^4 n_r (X_i^{rr} + X_i^{\bar{r}\bar{r}}), \quad S_i^z = \frac{1}{2} \sum_{r=1}^4 n_r (X_i^{rr} - X_i^{\bar{r}\bar{r}}), \quad (83)$$

can be expressed in terms of functions

$$K_{lm}^{(pq)}(\tau - \tau') = \langle TX_l^{pp}(\tau) X_m^{qq}(\tau') \hat{\sigma}(\beta) \rangle_{oc}. \quad (84)$$

The perturbation theory with respect to electron hopping term t_{ij} and the corresponding diagrammatic technique for Hubbard operators⁵⁸ were used to calculate these functions. The diagrammatic series were summed up in the GRPA, where the sequences of electron “loops” connected by semiinvariants (similarly to the case of the simplified PEM, see Sec. 3.1.1) or by vertices with the three fermion lines (such vertices appear only at $U \neq 0$) are taken into account.

The Fourier transforms $K^{(pr)}(\mathbf{q}, \omega_n)$ of functions (81) can be presented in the form^{25,26}

$$K^{pp'}(\omega_n, \mathbf{q}) = \beta \left\{ \bar{b}_{pp'}(\mathbf{q}) + \left[{}'\Pi(0, \mathbf{q}) \bar{b}(\mathbf{q}) \right]_{pp'} + \left[\bar{b}(\mathbf{q}) \Pi'(0, \mathbf{q}) \right]_{pp'} + \left[{}'\Pi(0, \mathbf{q}) \bar{b}(\mathbf{q}) \Pi'(0, \mathbf{q}) \right]_{pp'} \right\} \delta(\omega_n) + \Pi''_{pp'}(\omega_n, \mathbf{q}). \quad (85)$$

The first term in the right hand side of (85) is the “full” semi-invariant of the second order that satisfies the Dyson-type equation

$$\bar{b}_{pq} = \tilde{b}_{pq} + \left(\tilde{b} \Pi \bar{b} \right)_{pq}. \quad (86)$$

Here $\tilde{b}_{pq} = \langle X^{pp} X^{qq} \rangle_{oc}$ is the second-order semi-invariant calculated in mean-field approximation and the full “loop” contributions Π , Π' , ${}'\Pi$, Π'' are determined from the Bethe-Salpeter type equations

$$\begin{aligned} \Pi'' &= \Pi''_0 + \Pi''_0 \Pi' + {}'\Pi_0 \Pi'', \\ \Pi' &= \Pi'_0 + \Pi'_0 \Pi' + \Pi_0 \Pi'', \\ {}'\Pi &= {}'\Pi_0 + {}'\Pi_0 {}'\Pi + \Pi_0 \Pi'', \\ \Pi &= \Pi_0 + \Pi_0 {}'\Pi + \Pi'_0 \Pi. \end{aligned} \quad (87)$$

Zero-order polarization loops Π_0 , Π'_0 , ${}'\Pi_0$, Π''_0 are constructed of the single-electron Green's functions which are calculated in the Hubbard-I approximation (corresponding to the summation of chain fragments of diagrams).^{25,26} Loops Π'_0 , ${}'\Pi_0$, Π''_0 are determined only by intraband transitions whereas loop Π_0 is determined by the interband transitions as well

$$\Pi_0(mr, np) = \frac{1}{N} \sum_{\mathbf{k}} t_{\mathbf{k}} t_{\mathbf{k}+\mathbf{q}} \frac{n_+[\varepsilon_{mr}(\mathbf{k})] - n_+[\varepsilon_{np}(\mathbf{k} + \mathbf{q})]}{i\omega_n + \varepsilon_{mr}(\mathbf{k}) - \varepsilon_{np}(\mathbf{k} + \mathbf{q})}. \quad (88)$$

where $\varepsilon_{mr}(\mathbf{k})$ are determined in (78) and $n_+(\lambda)$ is Fermi distribution.

Numerical calculations of the static dielectric susceptibility $\chi_{\perp}(\mathbf{q}, 0)$ performed in Refs. [25, 75] along the $(0, 0) \div (\pi, \pi)$ line in the $2D$ Brillouine zone, revealed that, similarly to the above considered case $U = 0$, the essential feature of the model is the presence of divergences on the temperature dependencies of functions χ_n^{ss} and χ_{μ}^{ss} (Fig. 29). They appear in a certain range of the model parameter values. For $h > 0$ and $h < g$ such

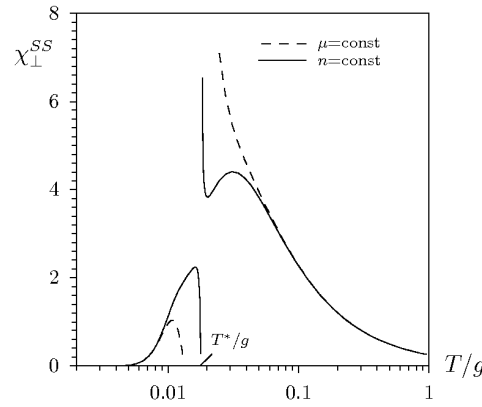


Fig. 29. Temperature dependence of χ^{ss} at $n = 0.95$ and $\mathbf{q} = 0$ ($U \rightarrow \infty$, $h/g = 1.05$, $W/g = 0.2$).

divergencies exist only at $\mathbf{q} = 0$ (Γ -point) and can be treated as the manifestation of the dielectric type instabilities which appear in the pseudospin subsystem (i.e., the system of anharmonic oscillators) under the influence of the effective interactions. As in the case of a simplified model, it means that the system can transform to another uniform phase. The corresponding phase diagram T^* vs n is shown in Fig. 30(a), where the lines limiting the stability region are plotted. For $0 < h < g$, besides the dielectric instability at Γ -point at $n \gtrsim 0$, the instability at $\mathbf{q} = (\frac{\pi}{a}, \frac{\pi}{a})$ (M -point) with respect to the charge ordering (double modulation) occurs (Fig. 30(b)). Such an instability is realized when the electron band (that corresponds to the lower Hubbard subband at $U \rightarrow \infty$) is nearly fully occupied.

The above mentioned divergences on the temperature dependencies and an increase of the dielectric susceptibility which takes place in the vicinity of $h = 0$ and $h = g$ values (for $U \rightarrow \infty$, $n < 1$) are connected, first of all, with the polarization contributions Π_0 from the electron transitions

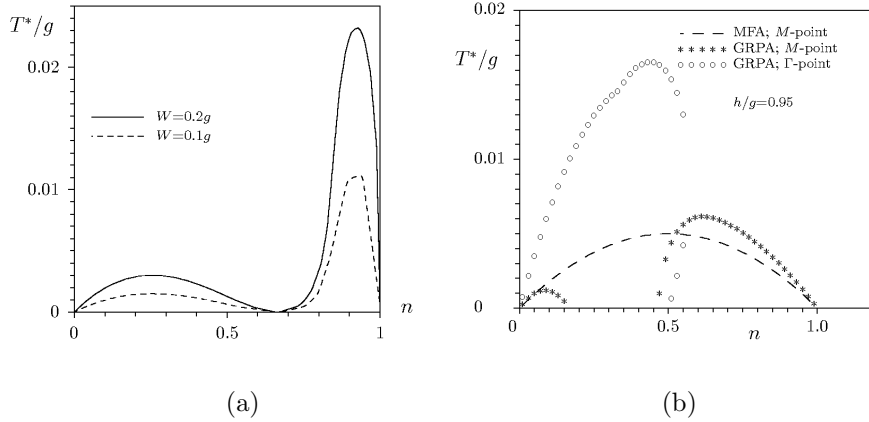


Fig. 30. Dependence of the instability temperature T^* on the electron concentration n in the cases $h > g$ and $0 < h < g$. (a) $U \rightarrow \infty$, $\Omega = 0$, $n/g = 1.05$ (dielectric instability, $\mathbf{q} = 0$). (b) $U \rightarrow \infty$, $\Omega = 0$, $n/g = 0.95$ (o o o – dielectric instability, $\mathbf{q} = 0$; * * * – instability with respect to CDW ordering, $\mathbf{q} = (\pi, \pi)$; dashed line shows the MFA results).

between hole subbands $(\tilde{4}\tilde{1})$ and $(\tilde{4}\tilde{1})$ (or $(\tilde{4}\tilde{1})$ and $(4\tilde{1})$). Just for $h \sim 0$ and $h \sim g$ these subbands come nearer to each other.

It should be noted that the results presented here for dielectric response of PEM in the $U \rightarrow \infty$ limit were used in Ref. [25] in describing the dielectric anomalies which have been observed in the high- T_c superconductors of the YBaCuO type at an early stage of investigations. In particular, the temperature dependence of χ_n^{ss} given in Fig. 29 was related to the one obtained experimentally for YBa₂Cu₃O_{7- δ} ⁹ where the similar behaviour of dielectric permittivity ϵ_c was found at the temperature near (and above) the point of the superconducting phase transition.

An interesting feature of the model at large values of U is the possibility of change of the electron concentration n under the influence of h . Such an effect can take place in the $\mu = \text{const}$ regime; this becomes possible when the chemical potential leaves (or enters) the energy subband²⁴ (Figs. 27 and 31(a)). The change of n is accompanied by the corresponding change of the pseudospin mean value (Fig. 31(b)). In the case of YBaCuO structure, this means that if μ moves inside the subband with the change of e.g. external electric field, then the electron concentration (average occupancy of states) in Cu₂O₂ layers changes. This causes a redistribution of O₄ ions in their equilibrium positions. All this may correspond to the so-called electric-field effect observed in HTSC compounds (see, for example, Ref. [77]).

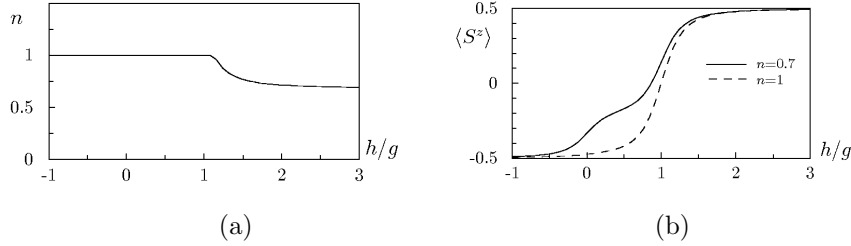


Fig. 31. Mean electron concentration n (a) and pseudospin mean value (b) as a function of h/g in the $\mu=\text{const}$ regime.

The obtained results show that in the $U \rightarrow \infty$ limit the PEM also exhibits a tendency to transform into another uniform or doubly modulated phase at low temperatures. It resembles the behaviour of the FK model in the strong coupling case.⁵⁷ The plots in Fig. 30 are given without the effect of phase separation. When the segregation on the regions with different n values takes place, the corresponding uniform phases or both the uniform and the modulated ones will coexist.

5. Two-Sublattice Pseudospin-Electron Model

Two-sublattice PEM^{35,36,37,38,76} appeared as a generalization of the usual PEM with the aim of more realistic description of the anharmonic subsystem of the apex oxygen ions in the YBaCaO type structures. In this case the pseudospin energy in the internal field is of the form $h \sum_i (S_{i1}^z - S_{i2}^z)$ that is the reflection of the mirror symmetry of the problem. Hamiltonian of the model is of the form³⁵

$$\begin{aligned}
 \hat{H} &= H_e + H_s + h_{l-s} + H_{s-s}, \\
 H &= H_e + H_s + H_{e-s} + H_{s-s}, \\
 H_e &= -\mu \sum_{n,s} (n_{n1}^s + n_{n2}^s) + U \sum_n (n_{n1}^\uparrow n_{n1}^\downarrow + n_{n2}^\uparrow n_{n2}^\downarrow) \\
 &\quad + \sum_{ij} \sum_{s\alpha} t_{ij} a_{is\alpha}^+ a_{js\alpha}, \\
 H_s &= -h \sum_n (S_{n1}^z - S_{n2}^z) - \Omega \sum_n (S_{n1}^x + S_{n2}^x), \\
 H_{e-s} &= g \sum_{n,s} (n_{n1}^s S_{n1}^z - n_{n2}^s S_{n2}^z),
 \end{aligned} \tag{89}$$

$$H_{s-s} = -J \sum_n S_{n1}^z S_{n2}^z - \frac{1}{2} \sum_{n,n'} \sum_{\alpha,\beta} J_{nn'}^{\alpha\beta} S_{n\alpha}^z S_{n\beta}^z.$$

Here, $n_{n\alpha}^s$ and $S_{n\alpha}^z$ are operators of the electron occupation number ($S = \uparrow, \downarrow$) and pseudospin, respectively, in the n -th unit cell ($\alpha=1,2$ corresponds to the two apex oxygen O_4 in the cell). Additionally to the term H_{e-s} describing the interaction between electrons and pseudospins, the direct interaction H_{s-s} between pseudospins is included; the $JS_{n1}^z S_{n2}^z$ interaction within the one-cell clusters is separated. Hamiltonian (89) is invariant with respect to the particle-hole transformation: $n_{n\alpha}^s \rightarrow 1 - n_{n\alpha}^s$, $h \rightarrow 2g - h$, $\mu \rightarrow -\mu - U$.

Thermodynamics of the system described by Hamiltonian (89) without a term related to the electron transfer was studied in Refs. [35, 36]. The mean-field approximation combined with the exact treatment of interactions within the one-cell clusters was used. For this purpose the single-clusters basis of states $|R_i\rangle \equiv |n_{i1}^\uparrow, n_{i1}^\downarrow, n_{i2}^\uparrow, n_{i2}^\downarrow\rangle \oplus |S_{i1}^z, S_{i2}^z\rangle$, which consist of sixty-four state vectors, was introduced. In such a way the grand canonical potential Φ_{MF} and the mean values $\langle S_\alpha^z \rangle$ and $\sum_s \sum_{\alpha=1}^2 \langle n_{n\alpha}^s \rangle = n$ were calculated.³⁵

Instead of the $\langle S_\alpha^z \rangle$ parameters, we can use their linear combinations: $\eta = \langle S_1^z + S_2^z \rangle$ (the order parameter for the ordered ferroelectric-like phase) and $\xi = \langle S_1^z - S_2^z \rangle$ (the parameter which is responsible for the in-phase reorientation of both pseudospins in the unit cell). In the regime $\mu = \text{const}$ we obtain the equations for η and ξ from the condition of the minimum of the grand canonical potential Φ_{MF}

$$\begin{cases} (\frac{\partial \Phi_{MF}}{\partial \eta})_\mu = 0, \\ (\frac{\partial \Phi_{MF}}{\partial \xi})_\mu = 0. \end{cases} \quad (90)$$

$$\begin{aligned} \Phi_{MF} = & \frac{1}{4} \{ (J_{11} + J_{12})\eta^2 + (J_{11} - J_{12})\xi^2 \} \\ & - T \ln \left[2 \left\{ e^{\beta \frac{J}{4}} \cosh \beta \frac{(J_{11}+J_{12})\eta}{2} + e^{-\beta \frac{J}{4}} \cosh \beta \left(h + \frac{(J_{11}-J_{12})\xi}{2} \right) \right\} \right. \\ & + 8e^{\beta\mu} \left\{ e^{\beta \frac{J}{4}} \cosh \beta \frac{(J_{11}+J_{12})\eta}{2} \cosh \beta \frac{g}{2} + e^{-\beta \frac{J}{4}} \cosh \beta \left(h + \frac{(J_{11}-J_{12})\xi}{2} - \frac{g}{2} \right) \right\} \\ & \left. + 8e^{2\beta\mu} \left\{ e^{\beta \frac{J}{4}} \cosh \beta \frac{(J_{11}+J_{12})\eta}{2} + e^{-\beta \frac{J}{4}} \cosh \beta \left(h + \frac{(J_{11}-J_{12})\xi}{2} - g \right) \right\} \right]. \end{aligned} \quad (91)$$

In the case $n = \text{const}$ the condition of the minimum value of the free energy

$F_{MF} = \Phi_{MF} + \mu n$, supplemented by the equation for chemical potential

$$-\frac{\partial \Phi_{MF}}{\partial \mu} = n,$$

was used to determine the thermodynamically stable equilibrium states.

When the set of equations (90) has a non-zero solution for η and the corresponding thermodynamic potential has a minimum, then our system is in the polar (ferroelectric) phase. The obtained phase diagrams in the $\mu = \text{const}$ case^{35,36} are shown in Fig. 32 (all parameters are normalized here by $J_{11} + J_{12} > 0$). One can see that at $\frac{J_{11}-J_{12}}{J_{11}+J_{12}} = -1$ (the case of pseudospin-pseudospin interaction between different sublattices only) the phase transition into ferroelectric phase is of the second order. The presence of the intra-sublattice interaction leads to the possibility of change of the phase transition order and the appearance of tricritical points. An increase of the $\frac{J_{11}-J_{12}}{J_{11}+J_{12}}$ parameter causes the narrowing of the ferroelectric region; its width is also proportional to J . At $J = 0$, $J_{12} = 0$ the model transforms into the one-sublattice PEM; the ferroelectric phase disappears and we have the first-order phase transition with zero value of the order parameter η and a sharp change of parameter $\xi = \langle S_1^z - S_2^z \rangle$.

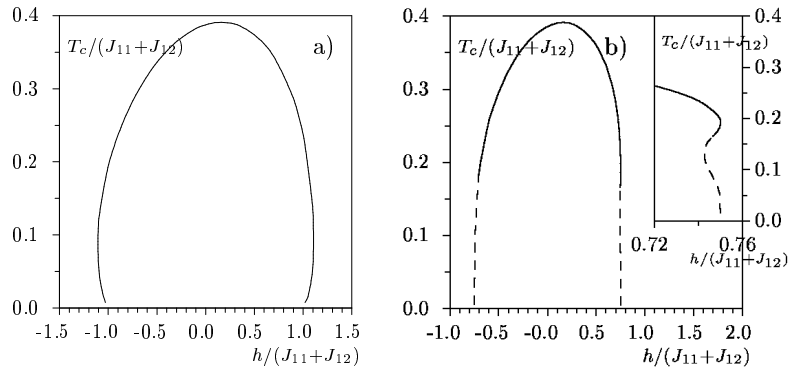


Fig. 32. (T_c-h) phase diagrams at different values of parameter $J_{11}-J_{12}$ in the regime $\mu = \text{const}$: a) $\frac{J_{11}-J_{12}}{J_{11}+J_{12}} = -1$, b) $\frac{J_{11}-J_{12}}{J_{11}+J_{12}} = 0$. Other parameters: $J/(J_{11} + J_{12}) = -1$, $g/(J_{11} + J_{12}) = 1$, $\mu/(J_{11} + J_{12}) = -1$. The phase transitions can be of the second (solid lines) or of the first order (dotted lines).

In the $n=\text{const}$ regime, the region of h values at which the ferroelectric phase exists becomes broader. The corresponding phase diagrams are shown in Fig. 33 at different values of long range interaction $J_{\alpha\beta} = \sum_{n'} J_{nn'}^{\alpha\beta}$ and

fixed concentration $n = 0.4$.

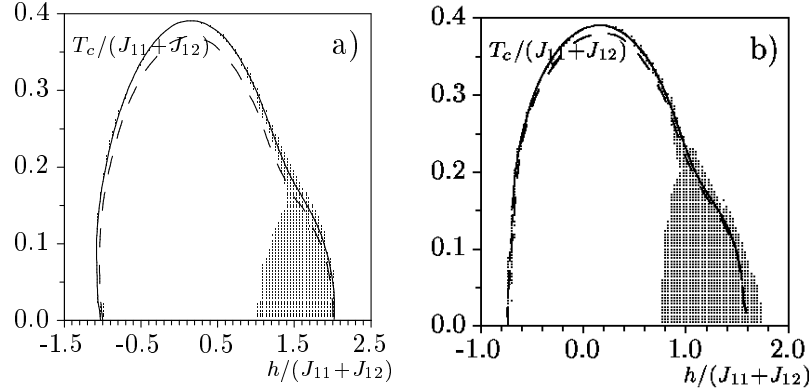


Fig. 33. The h dependence of the temperature of ferroelectric phase transition T_c at different values of parameter $J_{11} - J_{12}$ in the regime $n = \text{const}$: a) $(J_{11} - J_{12})/(J_{11} + J_{12}) = -1$, b) $(J_{11} - J_{12})/(J_{11} + J_{12}) = 0$. Other parameters: $J/(J_{11} + J_{12}) = 1$, $g/(J_{11} + J_{12}) = 1$, $n = 0.4$. Solid lines and dashed lines represent the second order and the first order phase transitions, respectively. The widely spaced dashed line corresponds to a one-loop approximation. Dots represent a separation area.

For comparison, there are also shown the phase transition lines obtained in the so-called one loop-approximation (in which the higher order corrections to the MFA described by two-tailed diagrams³⁶ are taken into account). In the areas marked by points, the system is separated into two regions with concentrations n_1 and n_2 ($n_1 < n < n_2$). Also, one can notice that phase separation takes place near the border of stability region of two phases (the ordered phase with nonzero polarization and the disordered one). That is why the ordered phase spreads wider and extends up to the edge of the separated area. Fig. 34 illustrates such a behaviour. Here the dashed lines represent the region of ferroelectric type instabilities. These lines would separate the ferroelectric phase if there were no phase separation. Figure 34(b) also shows that at a fixed value of asymmetry parameter h at concentration $n < 0.75$ (at low temperature), the ordered phase is possible only due to the phase separation.

Now, let us focus briefly on the effect of electron transfer. As above, we restrict ourselves to the limit $U \rightarrow \infty$. The case is considered, when the chemical potential is placed in the region of energy subbands ($\alpha = 1, 2$)

$$\varepsilon_{\alpha}^{31}(\mathbf{k}) = \varepsilon_{\alpha}^{41}(\mathbf{k}) = -(-1)^{\alpha} \frac{g}{2} + t_{\mathbf{k}} \langle X_{\alpha}^{44} + X_{\alpha}^{11} \rangle_0,$$

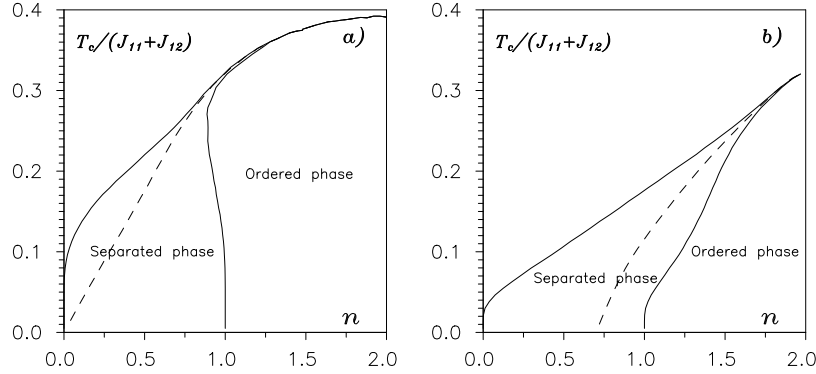


Fig. 34. Phase ($T-n$) diagram in a mean field approximation. The phase separation region is limited by solid lines. The dashed lines point to the region of ferroelectric instabilities. Parameters: $(J_{11} - J_{12})/(J_{11} + J_{12}) = 1$, $J/(J_{11} + J_{12}) = g/(J_{11} + J_{12}) = 1$; a) $h/(J_{11} + J_{12}) = 1$, b) $h/(J_{11} + J_{12}) = 1.35$.

$$\varepsilon_{\alpha}^{\tilde{3}\tilde{1}}(\mathbf{k}) = \varepsilon_{\alpha}^{\tilde{4}\tilde{1}}(\mathbf{k}) = (-1)^{\alpha} \frac{g}{2} + t_{\mathbf{k}} \langle X_{\alpha}^{\tilde{4}\tilde{4}} + X_{\alpha}^{\tilde{1}\tilde{1}} \rangle_0 \quad (92)$$

separated by the gap equal to g . The Hubbard-I approximation in which the expressions (92) are given here, was improved in Ref. [38] by the mean-field corrections (being of the form of the loop-like inclusions) to the electron Green's functions. Thus, renormalization of spectrum due to the shift of subbands dependent on electron concentration was taken into account. Besides, the mean values of Hubbard operators in (92) were determined self-consistently; the free energy of the pseudospin-electron systems was calculated in the above described GRPA approach. The pseudospin part of the two-sublattice Hamiltonian was taken in the MFA.

Figure 35 illustrates the effect of electron subsystems on the shape of the phase diagram. With respect to the standard Mitsui model (which corresponds to the $g = 0$ and $t_{ij} = 0$ limit), the phase boundary becomes asymmetric and the region of the ferroelectric phase existence is shifted to the higher values of h . As it has already been noted, at $J_{12} = 0$, ferroelectric phase does not exist and only a discontinuous change of ξ on the transition line takes place. Such a transition also remains in the case when $J_{11} = 0$ and only the indirect interaction via electron subsystem is present.

The changes in electron spectrum (see Refs. [37, 38]) are demonstrated in Fig. 36(b). In the case shown in Fig. 36, when at $n = \text{const}$ the separation into ferroelectric and nonpolar phases takes place, the $\eta(n)$ and $\mu(n)$ dependencies indicate that the ferroelectric phase appeared before the

separation. This is also supported by the presence of concavity in the free energy (dashed tangent lines in Fig. 36(c) link the points with concentration values n_1, n_2 and n_3, n_4 on which the separation takes place). Hence, there is a separation into paraelectric and ferroelectric phases at concentrations $n_1 < n < n_2$ and $n_3 < n < n_4$. The pure ferroelectric phase exists in the concentration range $n_2 < n < n_3$. The separation area in the (h, n) plane changes its shape depending on the t_{ij} value. In general, the electron transfer narrows the separation region.³⁷ The reverse effect also takes place: the electron spectrum is modified by a phase separation being sensitive to concentration value.

One can relate the phase transitions and ferroelectric type instabilities described by the herein considered two-sublattice PEM to the observed dielectric and thermodynamic properties of the YBaCuO-type superconducting crystals. In some experiments, YBa₂Cu₃O_{7- δ} was found to be both pyroelectric and piezoelectric, implying the existence of macroscopic polarization directed along the c-axis.⁷⁸ The possibility of the existence of the ferroelectric-like phase was not, nevertheless, unambiguously confirmed. In the two-sublattice PEM the ordered polar phase is present in a rather restricted region of the model parameter values, where the ground state is degenerated; for example, its width along the h -axis is determined by the interaction constant between the pseudospins (describing apical O₄ ions) within the unit cell cluster. In this connection, it should be mentioned

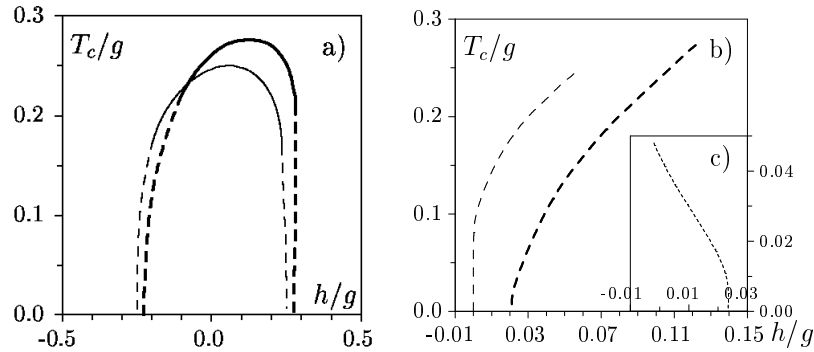


Fig. 35. Dependence of temperature of the phase transition T_c on the parameter h at different values of interaction parameters J_{11} and J_{12} in the regime $\mu = \text{const} = -g$. Thick lines correspond to the case $t_{ij}/g = 0.2$; thin lines correspond to the case $t_{ij} = 0$. a) $J_{11} = J_{12} = g/2$, b) $J_{11} = g, J_{12} = 0$. c) $J_{11} = J_{12} = 0, t_{ij}/g = 0.2$. Phase transitions are either of the second order (solid lines) or of the first order (dashed lines).

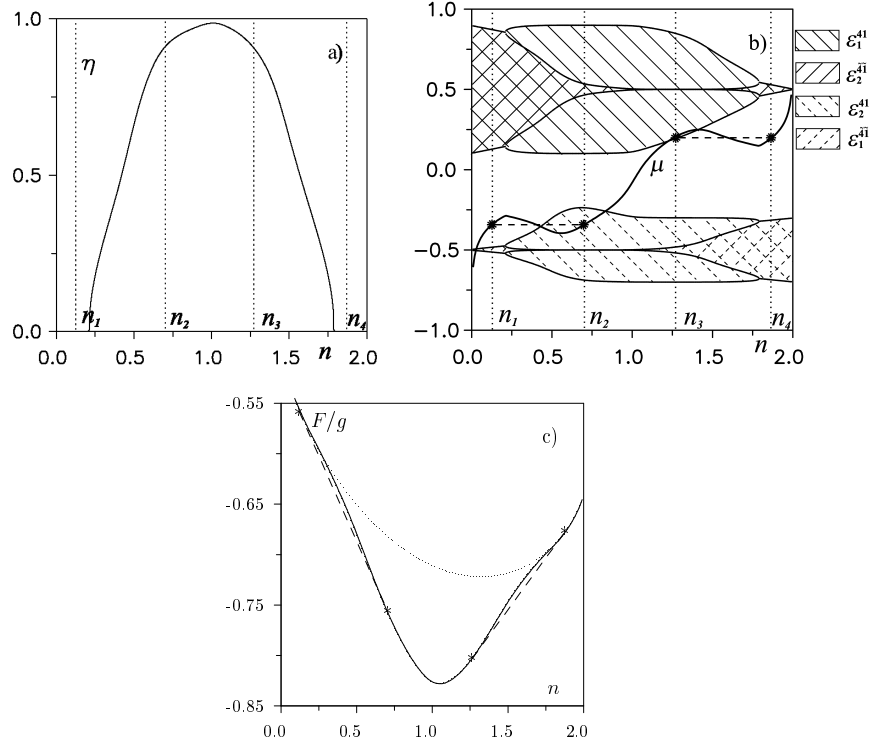


Fig. 36. Dependence of the order parameter η (a), band spectrum (b), and free energy (c) on electron concentration. The parameter values are: $J_{11} = J_{12} = g/2$, $T/g = 0.1$, $t_{ij}/g = 0.1$, $h/g = 0.5$.

that presence of the oxygen vacancies in the chain element of structure at $\delta > 1$ effectively influences the value of field h .⁷⁹ In its turn, instability with respect to the polar phase appearance can show up only at a certain nonstoichiometry (at certain values of parameter δ).

The phase separation in the two-sublattice case is also related to the real structure of the $\text{YBa}_2\text{Cu}_3\text{O}_{7-\delta}$ crystal. Besides the question of microscopic nature of the so-called “stripe phases” there is a problem of the genesis of structural inhomogeneities in a single crystal of the YBaCuO type observed in the experiments using Raman spectroscopy⁶ and mesoscopic structural investigations.⁸⁰ The results obtained within the model approach show the possibility of the Mitsui - type (due to both direct and indirect, via conducting electrons, interactions between anharmonic structure units) mechanism of the mentioned instabilities.

6. Conclusions

The present investigations of thermodynamics and energy spectrum of the PEM show a variety of phases and phase transitions. Depending on the thermodynamic equilibrium regimes, they manifest themselves as (i) transitions between different uniform phases, or between uniform and modulated phases, with the commensurate or incommensurate period of modulation (in the $\mu=\text{const}$ regime) or as (ii) transitions into phase separated states (in the $n=\text{const}$ regime). The latter takes place when at $\mu=\text{const}$, the corresponding phase transition is of the first order. Such phase transitions can be realized at the change of temperature T , field h , chemical potential μ (in the case (i)) and other parameters of the model. The corresponding phase diagrams are built in case of strong or weak coupling ($g \gg W$ and $g < W$, respectively).

A microscopic reason for phase transitions in standard PEM (without a direct pseudospin-pseudospin interaction) is related to the indirect effective coupling between pseudospins arising due to electron transfer and possessing a dynamic character. The form of such coupling depends on the electron concentration, temperature and the model parameter values. Consequently, the modulated phase appears at intermediate values of μ (this corresponds to the electron occupation near half-filling) both at strong and at weak coupling. However, the formation mechanisms of the effective interaction are different in these cases.

The two-sublattice PEM is a special case, close to the real HTSC systems of the YBaCuO type. The phase transitions described here, connected with the appearance of the ferroelectric state or with the jump-like change of the mutual orientation of pseudospins in sublattices, can have a relation to the segregation or bistability phenomena as well as to the development of ferroelectric-type instabilities in the mentioned systems.

The analysis carried out in the weak coupling case elucidates the role of the transverse field Ω (having a meaning of the tunneling-like splitting parameter) in the obtained picture of phase transitions. As a whole, a topology of the phase diagrams does not change at $\Omega \neq 0$ in comparison with the case $\Omega = 0$. The critical temperatures (including T_{SC}) decrease with Ω . In the case of DOS with logarithmic singularity (at dimensionality $d = 2$) a peculiar effect is revealed: the critical temperature remains finite at any large values of Ω (tending to zero at $\Omega \rightarrow \infty$, exclusively). This is the difference with respect to the behaviour of the systems with direct interaction (e.g., Ising model with transverse field). The important property is that at

$\Omega \neq 0$ the superconducting phase can appear in the PEM. Such a phase competes with the modulated one and is stable at the electron occupancy near the upper (or lower) edge of the electron band.

As is seen from the results obtained in DMFT for the simplified model, the structure of electron spectrum of the PEM is different in cases $g \gg W$ and $g < W$: the split subbands due to interaction (even at $U = 0$) or a single band, respectively. The similar spectrum is obtained in the approximations, based on the Hubbard-I scheme (e.g. GRPA) in the first case or the Hartree-Fock approach in the second one. As was shown by Zeyher, Kulić, and Gehlhoff,^{81,82,83} GRPA keeps in a systematic way all terms of the leading order of a so-called $1/N$ expansion, where N is the local spin component number on a lattice site. Though such approximations do not adequately reproduce all the features of spectrum, the obtained phase diagrams are in a good agreement with the ones constructed in DMFT. An interesting feature of spectrum is that there exists a critical value of g : at $g > g_c$ a gap appears (in the case of simplified PEM) and a metal-insulator type transition takes place.

Pseudospin-electron model (PEM) can be considered as a generalization of the Falicov-Kimball (FK) model to the case of different thermodynamic equilibrium regimes as well as an extension of the latter model due to the inclusion of the pseudospin dynamics and the Hubbard type correlations. The PEM possesses a similar variety of phase transitions but there are differences in the conditions of their realization and in the criteria of the appearance of different phases. In the above considered cases such differences are discussed and a comparison with the results for the FK model is made.

From the point of view of theoretical studies, the investigations of the PEM are far from complete. Another interesting problem is connected with the thermodynamics of the PEM with electron transfer at $U \neq 0$ and $\Omega \neq 0$. The investigations performed revealed only the existence of instabilities connected with certain values of the wave vector \mathbf{q} but the phase diagrams determining the regions of existence of different phases have not been built so far. The intermediate coupling case ($g \sim W$), that was not adequately investigated even for the simplified PEM, calls for more detailed consideration. An important point is to complete the study of the collective excitation spectrum (connected with pseudospin reorientation, electron transitions and polaron effect) and the dynamic susceptibility. Among the possible generalizations of the model, one can note an extension to the cases with the asymmetric electron transfer (in the spirit of the asymmet-

ric Hubbard model) and with pseudospin $S > 1/2$. They appear to be quite promising in connection with investigations of the ionic transport based on the lattice models as well as in the study of the ion intercalation processes (see e.g. Ref. 84 for a recent development in this field).

Acknowledgements

The author is grateful to A. Shvaika and T. Mysakovych for reading the manuscript and technical help.

References

1. K. A. Müller, Z. Phys. B **80**, 193 (1990).
2. S. Conradson and I. D. Raistrick, Science **243**, 1340 (1989).
3. J. Mustre de Leon, S. D. Conradson, L. Batistic, A. R. Bishop, I. D. Raistrick, M. C. Aronson, and F. H. Garzon, Phys. Rev. B **45**, 2447 (1992).
4. D. Mihajlovic and C. M. Foster, Solid State Commun. **74**, 753 (1990).
5. G. Ruani, C. Taliani, M. Muccini, K. Conder, E. Kaldis, H. Keller, D. Zech, and K. A. Müller, Physica C **226**, 101 (1994).
6. M. N. Iliev, V. G. Hadjiev, and V. G. Ivanov, Journ. Raman Spectr. **27**, 333 (1996).
7. N. Poulakis, D. Palles, E. Liarokapis, K. Conder, E. Kaldis, and K. A. Müller, Phys. Rev. B **53**, R534 (1996).
8. L. R. Testardi, W. G. Moulton, H. Matias, H. K. Ng, and C. M. Rey, Phys. Rev. B **37**, 2324 (1988).
9. V. Müller, C. Hucho, and D. Maurer, Ferroelectrics **130**, 45 (1992).
10. J. Mustre de Leon, I. Batistic, A. R. Bishop, S. D. Conradson, and S. A. Trugman, Phys. Rev. Lett. **68**, 3236 (1992).
11. J. Ranninger and U. Thibblin, Phys. Rev. B **45**, 7730 (1992).
12. A. P. Saiko and V. E. Gusakov, JETP **108**, 757 (1995).
13. P. Schweiss, W. Reichardt, M. Braden, G. Collin, G. Heger, H. Claus, and A. Erb, Phys. Rev. B **49**, 1387 (1994).
14. C. Ambrosch-Draxl and P. Knoll Physica B **194-196**, 2091 (1994).
15. J. Röhlér, in: *Materials and Crystallographic Aspects of HT_c -superconductivity*, edited by E. Kaldis (Kluwer, Dordrecht, 1994), p. 353.
16. R. J. Cava and A. W. Hewat, Physica C **C165**, 419 (1990).
17. J. R. Hardy and J. W. Flocken, Phys. Rev. Lett. **60**, 2191 (1988).
18. A. Bussman-Holder, A. Simon, and H. Büttner, Phys. Rev. B **39**, 207 (1989).
19. N. M. Plakida, Physica Scripta **29**, 77 (1989).
20. J. E. Hirsch and S. Tang, Phys. Rev. B **40**, 2179 (1989).
21. N. M. Plakida and V. S. Udovenko, Mod. Phys. Lett. **B6**, 541 (1992).
22. M. Frick, W. van der Linden, I. Morgenstern, and H. Raedt, Z. Phys. B **81**, 327 (1990).
23. I. V. Stasyuk, A. M. Shvaika, and E. Schachinger, Physica C **213**, 57 (1993).
24. I. V. Stasyuk and A. M. Shvaika, Fiz. Nizk. Temp. **22**, 535 (1996).

25. I. V. Stasyuk and A. M. Shvaika, *Ferroelectrics* **192**, 1 (1997).
26. I. V. Stasyuk and A. M. Shvaika, *Condens. Matter Phys.* **3**, 134 (1994).
27. V. Koerting, Q. Yuan, P.J. Hirschfeld, T. Kopp, J. Mannhart, *Phys. Rev. B* **71**, 104510 (2005).
28. N. Pavlenko, T. Kopp, *Phys. Rev. B* **72**, 174516 (2005).
29. I. V. Stasyuk and A. M. Shvaika, *Journ. Phys. Studies*, **3**, 177 (1999).
30. I. V. Stasyuk, A. M. Shvaika, and K. V. Tabunshchyk, *Condens. Matter Phys.* **2**, 109 (1999).
31. I. V. Stasyuk, A. M. Shvaika, and K. V. Tabunshchyk, *Ukrainian Journ. of Phys.* **45**, 520 (2000).
32. I. V. Stasyuk and T. S. Mysakovich, *Journ. Phys. Studies* **5**, 268 (2001).
33. I. V. Stasyuk and T. S. Mysakovich, *Condens. Matter Phys.* **5**, 473 (2002).
34. T. S. Mysakovich and I. V. Stasyuk, *Ukrainian Journ. of Phys.* **49**, 607 (2004).
35. O. D. Danyliv and I. V. Stasyuk, *Condens. Matter Phys.* **7**, 163 (1996).
36. O. D. Danyliv, *Physica C* **309**, 303 (1998).
37. O. D. Danyliv and I. V. Stasyuk, *Condens. Matter Phys.* **5**, 523 (2002).
38. I. V. Stasyuk and O. D. Danyliv, *Phys. Stat. Sol.* **219**, 229 (2000).
39. Yu. A. Izyumov and B. M. Letfulov, *J. Phys.: Cond. Matter* **2**, 8905 (1990).
40. I. V. Stasyuk and T. S. Mysakovich, *Journ. Phys. Studies* **3**, 344 (1999).
41. I. V. Stasyuk and T. S. Mysakovich, *Physica C* **341-348**, 171 (2000).
42. T. S. Mysakovich and I. V. Stasyuk, *Condens. Matter Phys.* **7**, 347 (2004).
43. J. K. Freericks and V. Zlatic, *Rev. Mod. Phys.* **75**, 1333 (2003).
44. I. V. Stasyuk, R. Ya. Stetsiv, and Yu. V. Sizonenko, *Cond. Matter. Phys.* **5**, 685 (2002).
45. I. V. Stasyuk and Yu. I. Dublenych, *Phys. Rev. B* **72**, 224209 (2005).
46. W. Wagemaker, G. J. Kearby, A. A. van Well, H. Mutka, and F. M. Mulder, *J. Am. Chem. Soc.* **125**, 840 (2003).
47. V. Koerting, Qingshan Yuan, P. J. Hirschfeld, T. Kopp, and J. Mannhart, *Phys. Rev. B* **71**, 104510 (2005).
48. W. Metzner and D. Vollhardt, *Phys. Rev. Lett.* **62**, 324 (1989).
49. A. Georges, G. Kotliar, W. Krauth, and M. J. Rosenberg, *Rev. Mod. Phys.* **68**, 13 (1996).
50. W. Metzner, *Phys. Rev. B* **43**, 8549 (1991).
51. U. Brandt and C. Mielsch, *Z. Phys. B* **75**, 365 (1989); *ibid.* **79**, 295 (1990).
52. G. Baym and L. P. Kadanoff, *Phys. Rev.* **124**, 287 (1961); G. Baym, *Phys. Rev.* **127**, 1391 (1962).
53. E. Dagotto, *Rev. Mod. Phys.* **66**, 763 (1994).
54. V. J. Emery and S. A. Kivelson, *Physica C* **209**, 597 (1993); U. Löw, V. J. Emery, K. Fabricius, and S.A. Kivelson, *Phys. Rev. Lett.* **72**, 1918 (1994).
55. T. Mertelj, J. Demsar, B. Podobnik, I. Poberaj, and D. Mihailovic, *Phys. Rev. B* **55**, 6061 (1997).
56. I. V. Stasyuk and A. M. Shvaika, *Czech. J. Phys.* **46**, 961 (1996).
57. J. K. Freericks, *Phys. Rev. B* **47**, 9263 (1993).
58. P. M. Slobodyan and I. V. Stasyuk, *Theor. Math. Phys. USSR* **19**, 616 (1974); (*Teor. Mat. Fiz.* **19**, 423 (1974)).

59. Yu. A. Izyumov, F. A. Kassan-Ogly and Yu. N. Skryabin, *Field Methods in the Theory of Ferromagnetism* (Nauka, Moscow, 1974) (in Russian).
60. I. V. Stasyuk and Yu. Havrylyuk, *Condens. Matter Phys.* **2**, 487 (1999).
61. J. K. Freericks and R. Lemanski, *Phys. Rev. B* **61**, 13438 (2000).
62. J. K. Freericks, Ch. Gruber, and N. Macris, *Phys. Rev. B* **60**, 1617 (1999).
63. U. Brandt and C. Mielsch, *Z. Phys. B* **82**, 37 (1991).
64. B. M. Letfulov, *Eur. Phys. J.* **4**, 447 (1998); **11**, 423 (1999).
65. I. V. Stasyuk and A. M. Shvaika, *Acta Phys. Polon. A* **84**, 293 (1993).
66. J. K. Freericks, *Phys. Rev. B* **48**, 14797 (1993).
67. N. M. Plakida and V.S. Udovenko, *Sverkhpr. Fiz. Khim. Tekhn.* **5**, 775 (1992).
68. Yu. A. Izyumov, M. I. Katsnel'son and Yu. N. Skryabin, *Magnetism of Itinerant Electrons* (Nauka, Moscow, 1992)(in Russian).
69. J. K. Freericks, M. Jarrell, and D. J. Scalapino *Phys. Rev. B* **48**, 6302 (1993); *ibid.* **B50**, 403 (1994).
70. C. S. Owen and D. J. Scalapino, *Physica* **55**, 691 (1971).
71. W. P. Su, *Phys. Rev. B* **67**, 092502 (2003).
72. N. N. Bogolyubov, V. L. Aksenov, and N. M. Plakida, *Teor. Mat. Fiz.* **93**, 371 (1992) (in Russian).
73. I. V. Stasyuk and A. M. Shvaika, *Acta Phys. Polon. A* **85**, 363 (1994).
74. I. V. Stasyuk, A. M. Shvaika, and E. Schachinger, *Physica B* **194-196**, 1965 (1994).
75. I. V. Stasyuk and A. M. Shvaika, *Physica C* **235-240**, 2173 (1994).
76. I. V. Stasyuk, A. M. Shvaika, and O. D. Danyliv, *Molec. Phys. Rep.* **9**, 61 (1995).
77. X. X. Xi, C. Doughty, A. Walkenhorst, C. Kwon, Q. Li, and T. Venkatesan, *Phys. Rev. Lett.* **68**, 1240 (1992).
78. D. Mihailovic and A. J. Heeger, *Solid State Comm.* **75**, 319 (1990).
79. I. V. Stasyuk and O. V. Velychko, *Ukrainian Journ. of Phys.* **44**, 772 (1999).
80. V. M. Browning, *Phys. Rev. B* **65**, 2860 (1997).
81. M. L. Kulić, R. Zeyher, *Phys. Rev. B* **49**, 4395 (1994).
82. L. Gehlhoff, R. Zeyher, *Phys. Rev. B* **52**, 4635 (1995).
83. R. Zeyher, M. L. Kulić, *Phys. Rev. B* **53**, 2850 (1996).
84. F. Zhou, T. Maxisch, G. Ceder, *Phys. Rev. Lett.* **97**, 155704 (2006).

INDEX

- approximation
 - coherent potential (CPA), 6
 - generalized random phase (GRPA), 12
 - Hubbard-I, 8
 - mean-field, 26
 - Migdal-Eliashberg, 39
- charge density wave (CDW), 19
- correlation
 - electron U , 2
- density of states (DOS), 6
- dielectric
 - instability, 47
 - response, 47
 - susceptibility, 45
- equation
 - Bethe-Salpeter, 39
- function
 - Green's, 5
 - Matsubara, 35
 - Zubarev, 35
 - pair correlation, 15, 34
- Hamiltonian
 - Hubbard, 2
- model
 - Falicov-Kimball (FK), 4
 - Hubbard, 2
 - Mitsui, 53
 - pseudospin-electron (PEM), 2
 - simplified, 12
 - two-sublattice, 48
- phase
 - chess-board, 20
 - coexistence, 27
 - diagram, 8, 34
 - ferroelectric, 50
 - incommensurate, 36
 - separation, 10
 - transition
 - first-order, 8
 - Mott, 7
- point
 - spinodal, 36
 - tricritical, 32, 50
- pseudospin, 2
- response
 - “isolated”, 35
 - isothermal, 34
- spinodal, 36
- state
 - superconducting (SC), 38
- theory
 - dynamical mean field (DMFT), 5
 - tunneling splitting, 2, 27, 41
- YBaCuO-type superconducting
 - crystals, 2, 35